Chapter 3

Synthesis and Application of Functional Prussian Blue Nanoparticles; A Photo-Fenton Catalyst for Dye

3.1 INTRODUCTION

Industries like textiles, leather and food discharge huge quantity of toxic pollutants in the natural water source, which may affect living organism (Ameen et al., 2016; Banazadeh et al., 2016). Notably, a different type of synthetic dye inclosing chromophore structures causes severe problems to both flora and fauna (Matouq et al., 2014; Wang and Chu, 2011). In particular, xanthene dye Rhodamine B (RhB) is reported to be neurotoxic, mutagenic, carcinogenic, and irritates skin, eyes, and the respiratory tract (Combes and Haveland-Smith, 1982) even at their low quantity. Consequently, the complete removal of those above non-biodegradable organic dye from wastewater has been one of the substantial environmental issues. The role of heterogeneous photocatalysis has been widely accepted techniques for environmental purification. Photocatalytic degradation of Direct Red 80 processed via UV/TiO_2/H_2O_2 accomplished the complete degradation of pollutant (Mahmoodi et al., 2005). Further, designing of heterogeneous catalyst as Fenton-like reagent for dye degradation has gained great attentions (Calleja et al., 2005; Kan and Huling, 2009; Kasiri et al., 2008; Li et al., 2015b; Ramirez et al., 2007; Rodriguez et al., 2010). Heterogeneous Fenton like oxidation and photo-Fenton process, in the presence of iron (II, III) oxide and iron nanoparticles with oxidant H_2O_2, attributed the highest structural stability and catalytic activity of catalyst with respect to cationic and anionic dye (Shahwan et al., 2011; Xu et al., 2004; Xue et al., 2009).

The photodegradation of RhB was investigated over the gelatin/CuS/PVA nanocomposite justifying the solar-light-induced catalytic activity (Al-Kahtani et al., 2017). Advanced oxidation processes (AOPs) has been employed previously for the removal of chloroacetic acids and methyleneblue from the aqueous media (Aziz, 2019; Aziz et al., 2018). Prussian blue nanoparticles (PBN) and its analogues shows potential viability in practical applications due to their numerous important properties (Kawamoto et al., 2010; Wessells and Huggins, 2015). The photo-Fenton process mediated through Prussian blue (PB) had also been emphasized revealing effective role of alkali cation on dye degradation in real time (Liu et al., 2010). In addition, PB-modified Fe_2O_3 magnetic nanoparticles (PBMNPs) was explored as peroxidase-like catalyst to remove methylene blue organic pollutants from aqueous solution (Wang and Huang, 2011). Although, the role of PB has been documented in dye degradation limited the practical usability since the use of two precursors yielded the formation of PB that underwent agglomeration with time and thus severely restricting the nanogeometry available for catalytic application (Doumic et al., 2016).

Previously, an attempt has been made on the synthesis of PBN for the controlled conversion of single precursor potassium ferricyanide into PBN (Gotoh et al., 2007; Pandey and Pandey, 2013b), and subsequently includes the synthesis of nanoparticles in a homogeneous and heterogeneous matrix along with PdNP to tune the catalytic activity for practical applications (Pandey and Pandey, 2012b; Pandey et al., 2018b). Further tailoring the chemical reactivity of nanomaterials at the atomic level, through regular alternation, is one of the critical challenges in catalysis research during the recent time (Mostafa et al., 2010). As, the smaller nanoparticles provide a larger surface area that fascinating more dye molecules and enhancing their catalytic performance during dye degradation (Fosso-Kankeu et al., 2016). The current research has been attempted with the use of epoxy-functionalized alkoxysilanes in the presence of cyclic ketone which not only allowed the formation of PBN of the desired nanogeometry from a single precursor but also tended to transition in crystal morphology of the same with remarkable potential application in dye degradation based on photo-Fenton process in real time. The photo-Fenton process was observed to be precisely controlled through the use of processable PBN of controlled nanogeometry and crystal morphology that displayed remarkable finding on the degradation rate, which has been investigated and reported in this investigation.

The as-synthesized PBN is explored as a catalyst for RhB degradation under Room Temperature/Heating/UV/solar light irradiation. Since, PBN itself is structurally interesting and typically absorbs red light of spectrum (590 to 635 nm) and underwent intervalence charge transfer transitionfrom ferrous to ferric, Fe^{+II}-C → N-Fe^{+III}, that defines the band gap of their iron cyanide framework (Robin, 1962).

Consequently, it was found that solar light irradiation is the fastest and more effective for complete removal (100% degradation) of dye using PBN. Intropical countries, sunlight is abundantly available as a natural light source. Meanwhile, the photo-Fenton process may allow efficient and inexpensive route of dye degradation. The aforesaid PBN/H_2O_2 complex generated reactive radicals species via photo-Fenton process and displayed excellent catalytic activity against dye degradation in the acidic medium. EPR analysis was performed to identify the generated reactive oxygen species such as hydroxyl and superoxide radicals throughout the dye degradation. Various param- eters such as pH, concentration of catalyst, H_2O_2 content, and concentration of targeted dye (RhB) were investigated thoroughly to understand the impact of individual on degra- dation rate and efficiency. Besides, LC-MS was used to identify the degraded end productof RhB. Further, COD parameter was analysed to determine the extent of mineralization of the organic intermediates. Stability of the re-cycled catalyst was studied to observe the impact of degradation over it, at the end of process. In addition, photo-Fenton process was also employed over waste water to observe the process productivity in the presence ofother interfering substances. The present works aim to propose here a simple, highly effi- cient, and eco-friendly technology for photocatalytic degradation of RhB, mediated with PBN, in the presence of H_2O_2 for the very first time and attracted considerable attention for its identified non-toxic end product. This interesting link emerged the PBN based materials as a potent catalyst for the photocatalytic applications.

3.2 EXPERIMENTAL

3.2.1 Materials

2-(3,4-Epoxycyclohexyl)ethyltrimethoxysilane (EETMSi) with 97.0% assay, 5,5-Dimethyl- 1-pyrroline N-oxide (DMPO) with 97.0% assay, 2,2,6,6-Tetramethylpiperidine1-oxyl (TEMPO) with 98.0% assay, and Rhodamine B (RhB) with 95.0% assay were obtained from Sigma-Aldrich Chemical Co. India. Potassium ferricyanide was obtained from Merck, India. Hydrogen peroxide (assay percentage purity 30-32% v/v) was purchased from Fischer scientific (ACS certified). cyclohexanone (99.8% assay) was purchased from Pub- chem. All other chemicals used were of analytical grade and found from the commercial source. Milli-Q water was used throughout the experimental process.

3.2.2 Preparation of PBN

Four different size of PBN i.e.; PBN_1, PBN_2, PBN_3 and PBN_4 were synthesized through chemical reduction method using EETMSi and cyclohexanone. In a typical experiment, 100 μl of potassium ferricyanide (0.01M) was mixed thoroughly with 20 μl EETMSi (0.01 M, 0.05 M, 0.1 M and 0.5 M) and stirred for 5 minutes. Later, 20 μl of cyclohexanone (9.8M) was added to the resulting mixture under stirring condition. The resulting mixture was left to stand in an oven at 333 K resulting into four different blue coloured nano-dispersion at different concentrations of EETMSi i.e., (a) PBN_4 (0.5M), (b) PBN_3 (0.1M) (c) PBN_2 (0.05M) and (d) PBN_1 (0.01M) (Fig. 3.3).

3.2.3 Instrumentation

Zeta potential analysis were done using Zetasizer nano ZS90 (Malvern instrument). Before analysis, the mandatory sample was prepared by diluting corresponding nanopar- ticles into milli-Q water followed by ultrasonication. EPR of generated radicals were determined using the Bruker BioSpin instrument. Agilent Scientific Liquid Chromatography Mass-Spectrometry (LC-MS) instrument was used for identification of RhB degraded end product. Similarly, the alterations in surface area of catalyst (PBN), after their active participation, was examined by BET analysis. Prior to N_2 adsorption/desorption process the sample were degassed at 150 $^{\circ}$C for 5 hours.

3.2.4 Experimental setup and measurement of photon flux

The apparatus employed during the photodegradation of RhB consist of the light sources (Solar light/UV-light) and the Photo-reactor (glass pyrex). For the experiment, proceeded under UV-light, the germicidal power was kept fixed at 130 W and the reactor was placed at a fixed distance of 30 cm away from the energy-light source. The measured power intensity (irradiance) of the incident radiation at the optical glass reactor from that fixed distance (30 cm) was found to be 144 mW/cm^2. For the solar light experiment, actinometer (pyranometer) was used for quantification of solar irradiation that reached out to the glass pyrex. The measured photo irradiations were obtained using pyranometer for the particular time of range (Time-12.00 to 1.00 pm, Temperature-311 K in BHU during the month of March) was found to be 1200 W/m^2.

3.2.5 Photocatalytic assay of RhB using PBN

The photochemical degradation efficiency of RhB molecules was performed under the different conditions such as room temperature (RT), solar radiation, UV-lamp and in heating (333 K) circumstance. The as-synthesized $PBN_1/PBN_2/PBN_3/PBN_4$ was employed in 25 ml of RhB solution (10-50 ppm). Further, H_2O_2 was added to the reaction mixture under stirring condition. The corresponding mixture was stirred for 2 min to establish the equilibrium state between catalyst-H_2O_2-RhB. Once the system has reached the adsorption/desorption state of equilibrium, the non-degraded concentration of RhB measured at 0 min is taken to be an initial concentration of dye for the photocatalytic process. Then left were irradiated under RT/heating/UV-lamp/solar radiation. Periodically at every 5 min, 2 ml of the solution was withdrawn out of the reaction system, and their extent of degradation is evaluated using UV-Vis spectrophotometer via measuring the concentration of dye at 554 nm. The experiment under solar radiation was carried out during the summer season (March-April) between 11 am to 1 pm. All the reaction systems, which were selected for comparative degradation analysis through UV-Vis spectrum, were kept simultaneously (at similar time) under solar light. And later the spectrum of each sample was recorded immediately.

The wavelength of UV-light source (130 W) was in the range of 180-380 nm, as H_2O_2 shows a high molar absorption at 253 nm (UV-C region). After degradation, the final concentration of RhB was measured using UV-Vis spectrophotometer. The de-colourization percentage of RhB was calculated as follows.

$$\% D = (C_0 - C_t)/C_0 \times 100$$

Where C_0 is the initial and C_t is the final concentration of dye in solution after 't' time of photo-irradiation and %D is degradation efficiency.

3.2.6 EPR analysis of generated hydroxyl radical

The optimum amount of PBN (0.1 M, 20 μl) homogenous sol was dispersed in distilled water (2 ml) by ultrasonication. Later 10 μl of ethanolic solution of DMPO (100 mM) and TEMPO (100 mM) were mixed with the resultant nanodispersed sol followed by stirring. After adding desired amount of H_2O_2 to the reaction, the whole mixture was allowed to irradiate for 2 min under solar light. After completion of reaction, 1 ml of resultant sample was transferred in a quartz capillary tube and placed in the Electron Paramagnetic Resonance (EPR) spectrometer cavity for radical analysis. The magnetic field was set at 3420 G center field with sweep width of 1000 G and sweep time of 102 s. Signal channel was set to 5 number of the scan with mod. amplitude of 1 G and frequency 100 kHz.

3.2.7 Characterization and analysis of photo-Fenton catalyst

UV-spectrum

The UV-Vis spectroscopy displays a sharp peak at 420 nm for potassium ferricyanide ($K_3Fe(CN)_6$) and an intense and broad peak at 680 nm for PBN (Fig. 3.1). The successful conversion of potassium ferricyanide to PB was similarly accomplished through chemical reduction method via varying one component while keeping others fixed and their corresponding UV-Vis spectrum are recorded. Consequently, the optimum concentration of each reagent i.e., $K_3Fe(CN)_6$/EETMSi/ cyclohexanone were acquired to yield PBN; (I) Synthesis performed at different concentrations of 100 μl of $K_3Fe(CN)_6$ (a) 0.05 M (b) 0.04 M (c) 0.03 M (d) 0.02 M and (e) 0.01 M with constant EETMSi (20 μl, 0.05 M)

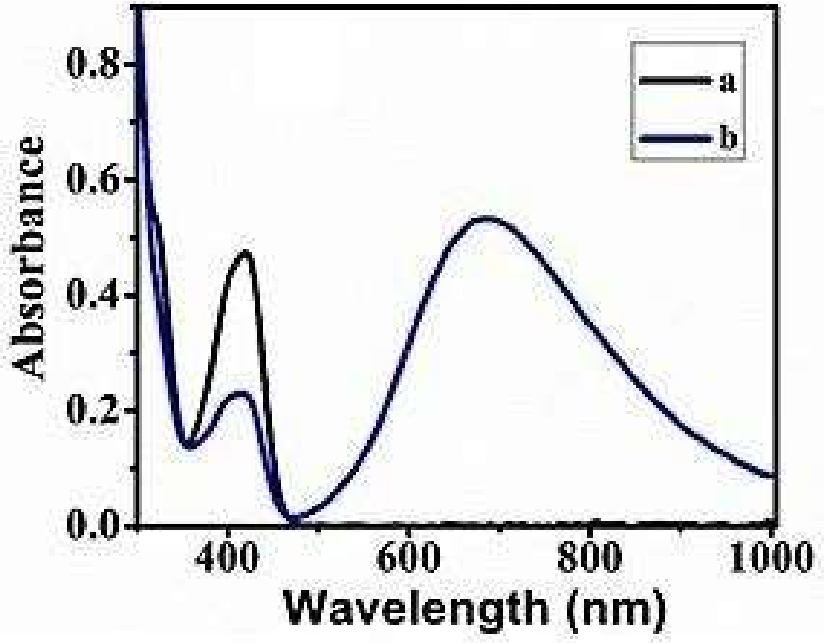

Figure 3.1: Recorded UV-Vis spectra of potassium ferricyanide (a) and synthesized PBN (b).

---

and cyclohexanone (20 μl, 9.8 M) concentration (Fig. 3.2 A). (II) Synthesis via varying amount of cyclohexanone (9.8 M); (a) 25 μl, (b) 20 μl, (c) 15 μl and (d) 10 μl; (e) 5 μl at constant EETMSi (20 μl, 0.05 M) and ferricyanide content (100 μl, 0.03 M) (Fig. 3.2 B). And (III) fabrication accomplished at different concentrations of 20 μl of EETMSi; (a) 0.5 M (b) 0.1 M (c) 0.05 M (d) 0.01 M with a fixed ferricyanide content (100 μl, 0.03 M) and cyclohexanone (20 μl, 9.8 M) (Fig. 3.3). The blue shift was observed while increasing EETMSi content with a decrease in size as well. Similarly, the effective concentration of as-synthesized PBN based on absorbance data was obtained to be; 9.70 mM/ml, 8.12 mM/ml, 7.25 mM/ml and 6.02 mM/ml for PBN_4 (Fig. 3.3 a), PBN_3 (Fig. 3.3 b), PBN_2 (Fig. 3.3 c), and PBN_1 (Fig. 3.3 d) respectively using relation: ($C=A/b\xi$), where $\xi = 3 \times 10^4$ M^{-1} cm^{-1}. The effective conversion of potassium ferricyanide into PBN based on UV-Vis spectroscopy (Fig. 3.3) was estimated between 58% - 87%.

XRD

The crystallinity of as prepared PBN has been exhibited by Powder XRD (P-XRD). The strong and sharp peak indexed at 2θ values of 17.42, 24.96, 35.43, 39.54, 43.54, 50.72, and

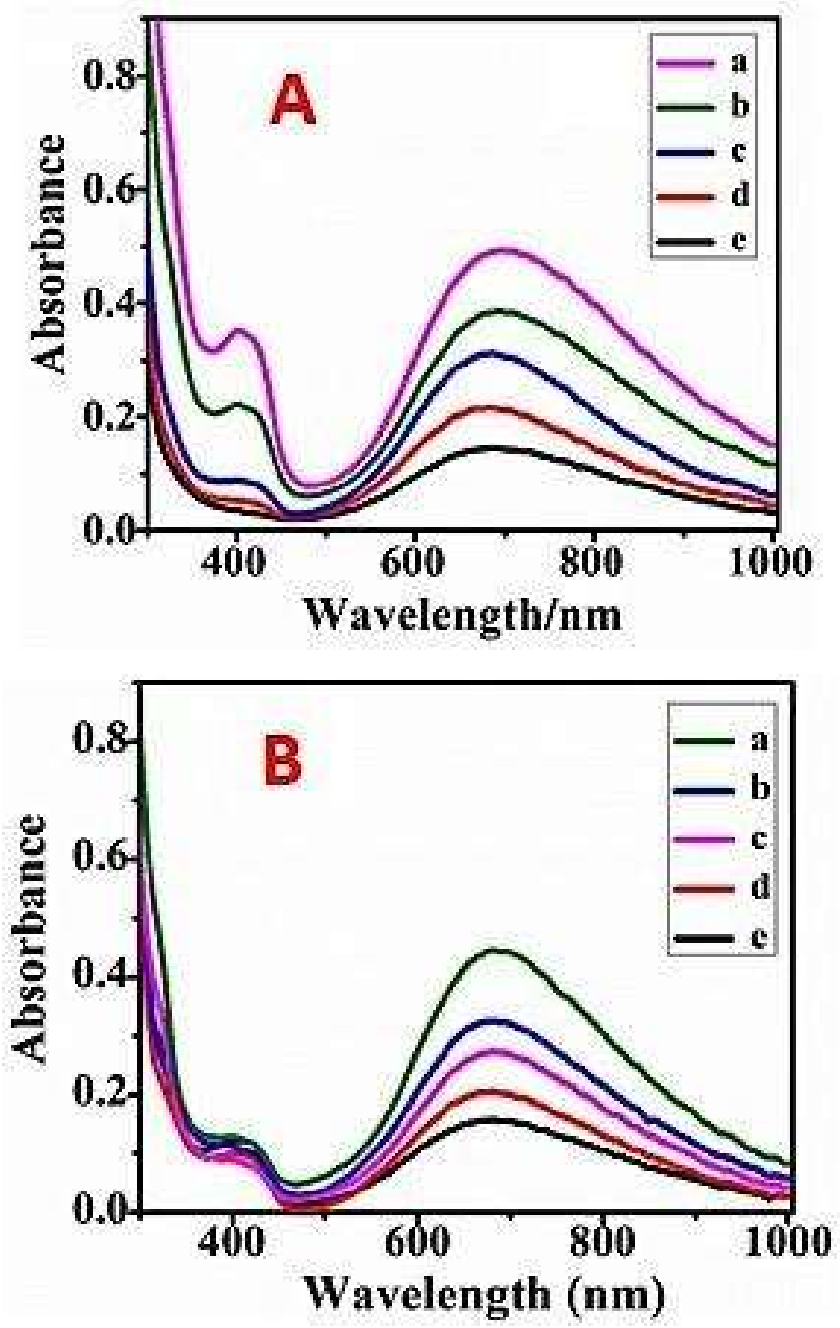

Figure 3.2: Recorded UV-Vis spectra of PBN synthesis (A) at different concentrations of 100 μl of ferricyanide; (a) 0.05 M (b) 0.04 M (c) 0.03 M (d) 0.02 M and (e) 0.01 M with constant EETMSi (20 μl, 0.05 M) and cyclohexanone (20 μl, 9.8 M) contents, and (B) via varying cyclohexanone amount; (a) 25 μl, (b) 20 μl, (c) 15 μl and (d) 10 μl; (e) 5 μlat constant EETMSi (20 μl, 0.05 M) and ferricyanide content (100 μl, 0.03 M).

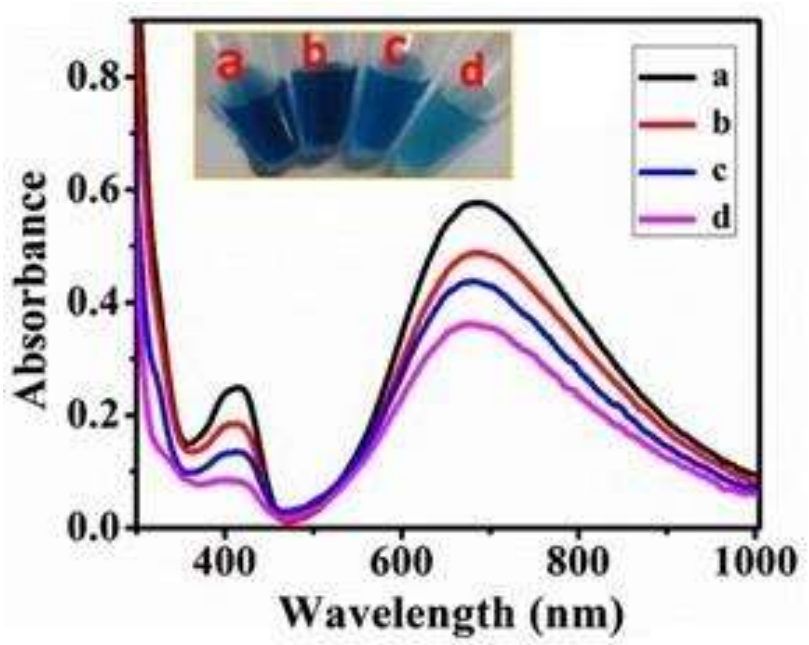

Figure 3.3: Spectrum recorded at different concentrations of 20 μl of EETMSi; (a) 0.5 M (b) 0.1 M (c) 0.05 M (d) 0.01 M with a fixed ferricyanide content (100 μl, 0.03 M) and cyclohexanone (20 μl, 9.8 M).

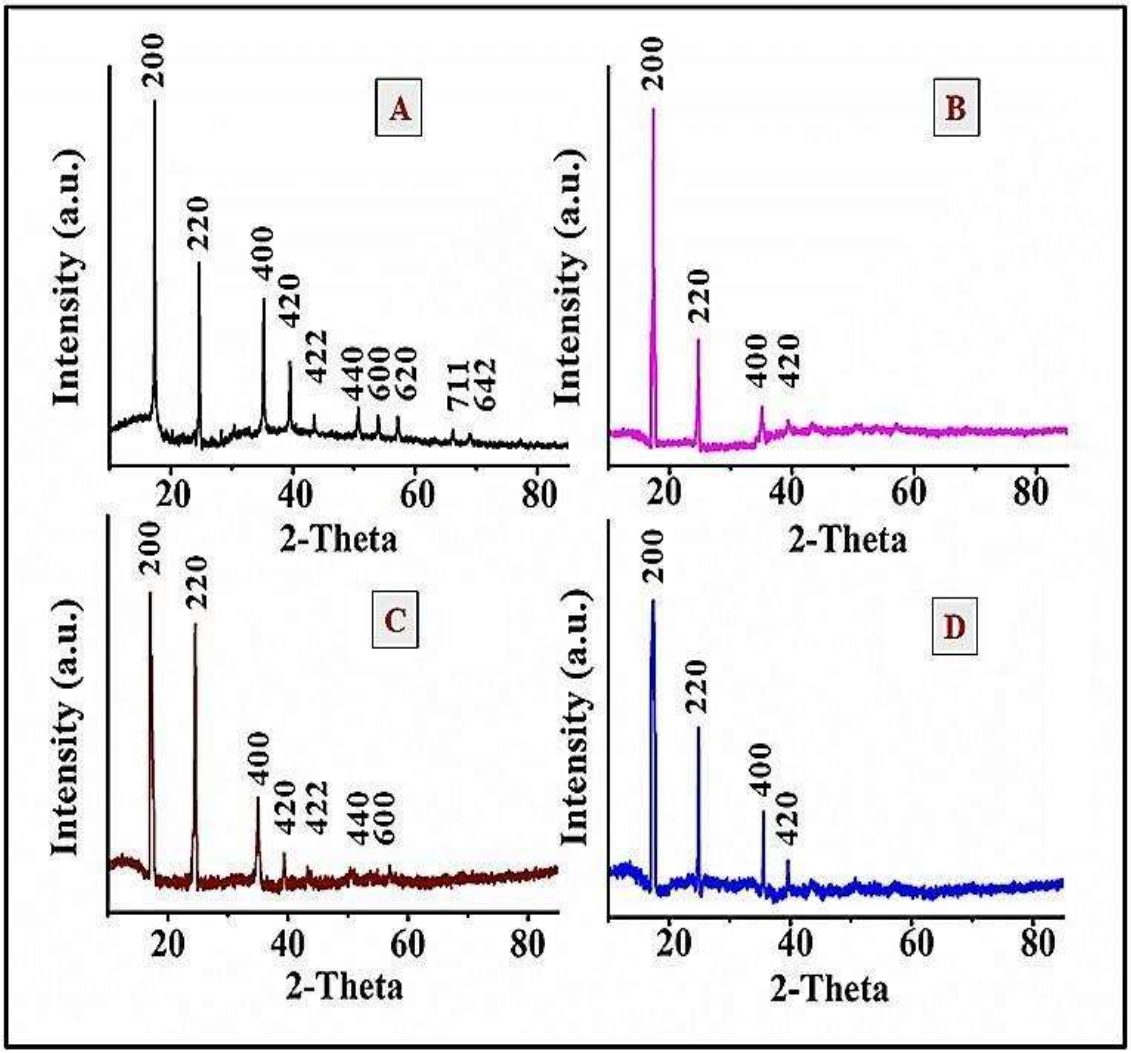

Figure 3.4: P-XRD of as prepared PBN_1 (A), PBN_2 (B), PBN_3 (C), and PBN_4 (D).

54.03 (as shown in Fig. 3.4(A,B,C,D)) assigned to (200), (220), (400), (420), (422), (440), and (600) planes, indicating face-centered cubic crystal lattice type structure (JCPDS no. 73-0687). The crystalline size of PBN_1,PBN_2, PBN_3, and PBN_4 were calculated using Scherrer's equation and found to be 52.3 nm, 42.8 nm, 26.5 nm, and 6.5 nm respectively.

FTIR spectrum of PBN

The prominent peak located at 2092 cm^{-1} in the IR spectrum (Fig. 3.5) resembled with the stretching mode of Fe(II)-C-N-(III)Fe moiety in PBN (Ayers and Waggoner, 1971). The broad band revealed at 3402 cm^{-1} and 1642 cm^{-1} in the spectrum correspond to OH-stretching and H_2O bending mode of the interstitial water molecule respectively within

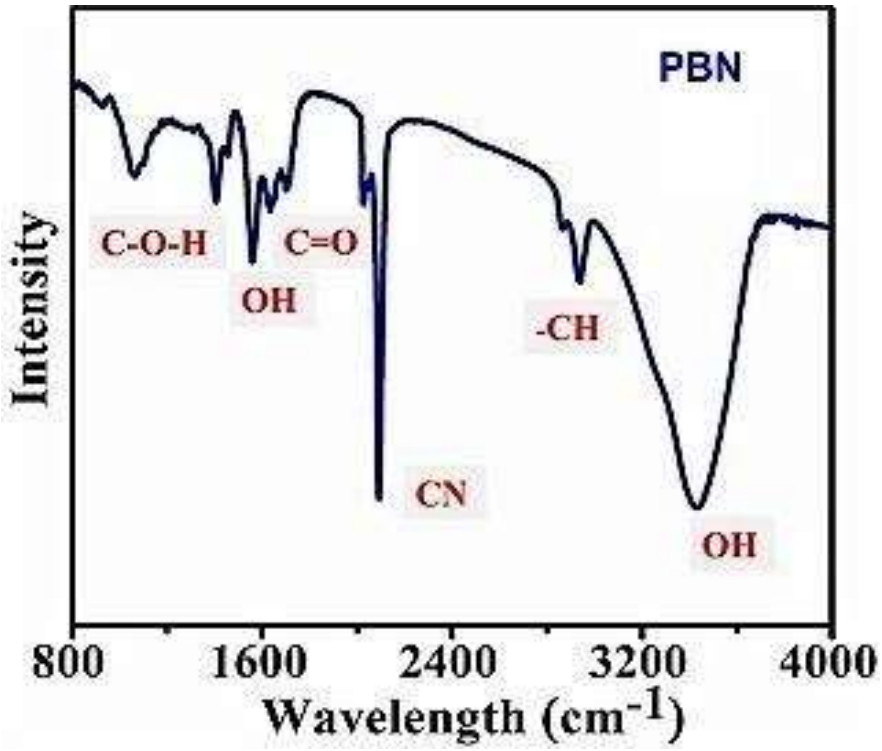

Figure 3.5: FTIR spectrum of as-synthesized PBN indicating functional species.

PBN lattice. Some additional vibration mode at 1587 cm^{-1} showed the formation of alkene derivative via active participation of EETMSi (Pandey et al., 2018a). The strong band shown near to 2890-2990 cm^{-1}, correspond to the sp^2 hybridized C-H stretching vibration in cyclohexanone. Indistinct peak at 1109 cm^{-1} and 891 cm^{-1} shows the active participation of alkoxysilane.

EDX

The strong peak observed in the EDX spectrum of PBN confirmed the presence of all required element Fe, C, N, Si, and O as displayed in Fig. 3.6. The prepared PBN sample revealed the weight percentage at 53.11 % of C, 18.88 % of N, 26.18 % of O, 1.79 % of Si, and 0.04 % of Fe. The EDX analysis was performed on carbon coated Cu grid.

TEM analysis

The HR-TEM images of PBN_1 (Fig. 3.7(A,B)), PBN_2 (Fig. 3.9(A,B)), PBN_3 (Fig. 3.11(A,B)) and PBN_4 (Fig. 3.13(A,B)) with different magnification clearly shows the

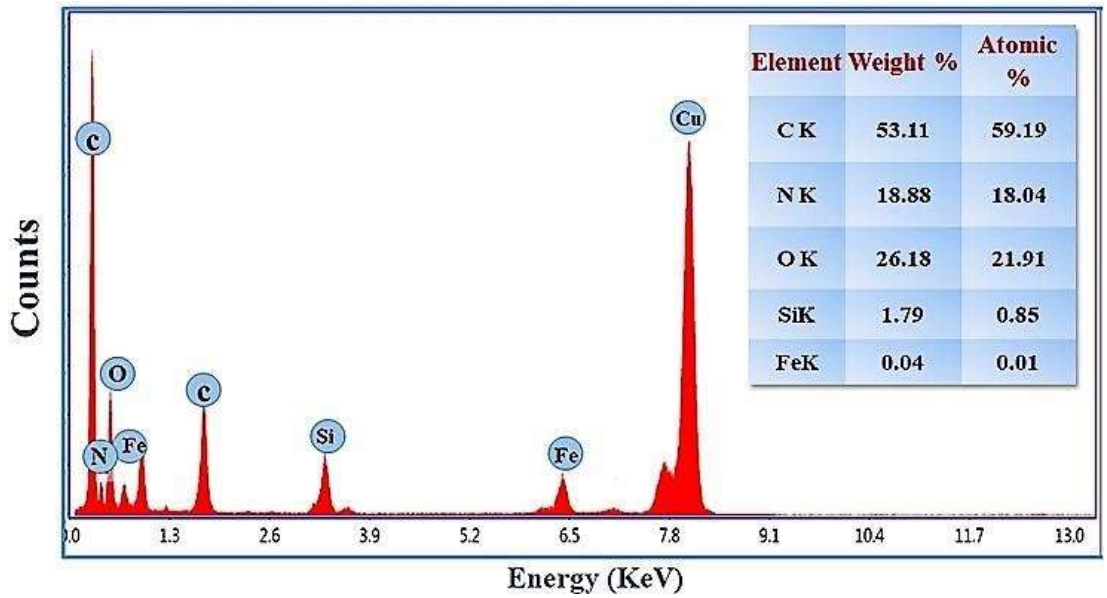

Figure 3.6: Elemental confirmation was characterized by EDX.

eventually distributed uniform nanocubes and nanospheres. It also displays that the morphology and size were changed from nanocubes to spherical one with less agglomeration dependent on alkoxysilane EETMSi concentration. To get further insight into nanostructure, the fringes of 0.416 nm (Inset of Fig. 3.7A, 3.9A, 3.11A and 3.13A), obtained from high-resolution TEM imaging clearly shows the presence of planes. Particularly, the lattice fringes (0.416 nm) of PBN correspond to the prominent head peak at $2\theta = 17.6$ can be indexed to the (200) plane. The different selected area electron diffraction (SAED) pattern shows the polycrystalline nature of PBN_1 (Fig. 3.8A), PBN_2 (Fig. 3.10A), PBN_3 (Fig. 3.12A), and PBN_4 (Fig. 3.14A). The resultant histograms of well-distributed particles of PBN_1 (Fig. 3.8B), PBN_2 (Fig. 3.10B), PBN_3 (Fig. 3.12B), and PBN_4 (Fig.3.14B) confirmed the mean size dimension ranges from 13 to 53 nm. EETMSi successively plays an influential role over the size and nanogeometry of particles as a function of their content, evidenced through resultant TEM analysis.

XPS analysis

The XPS data (Fig. 3.15) indicated the occurrence of both Fe (II) and Fe (III) species in as-synthesized PBN. The peaks centred on binding energy of 721.87 eV and 708.64 eV corresponds to Fe $2p_{1/2}$ and Fe $2p_{3/2}$ respectively proved the characteristic Fe^{+2} moiety

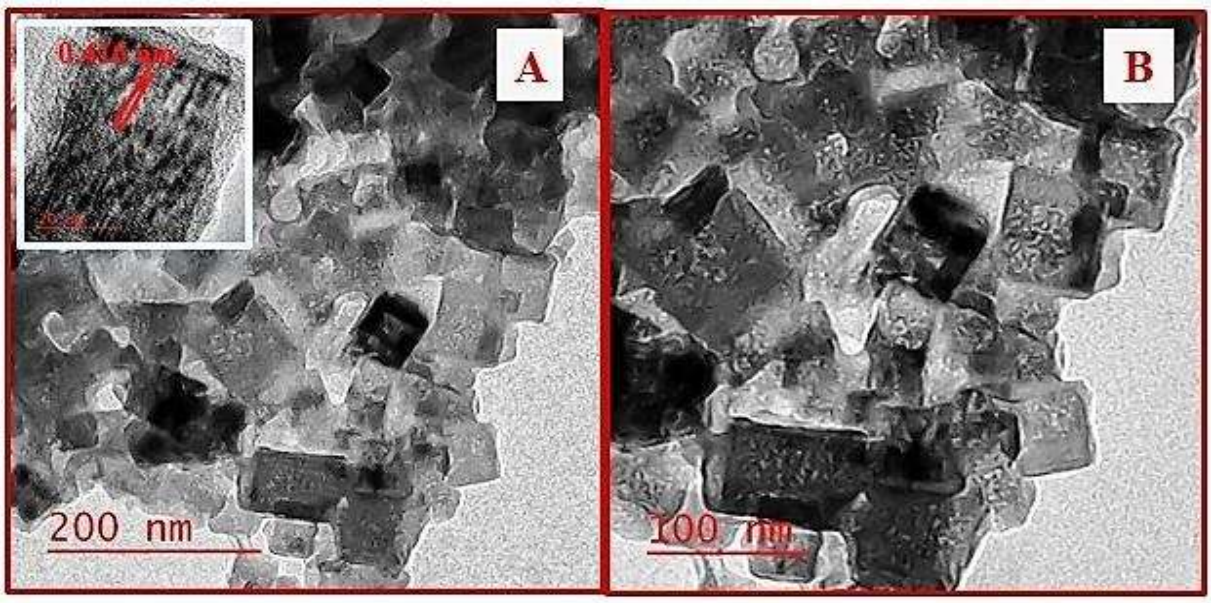

Figure 3.7: TEM images of PBN_1 (A,B), and the image shown in inset of (A) displayed lattice fringes of the corresponding nanoparticles.

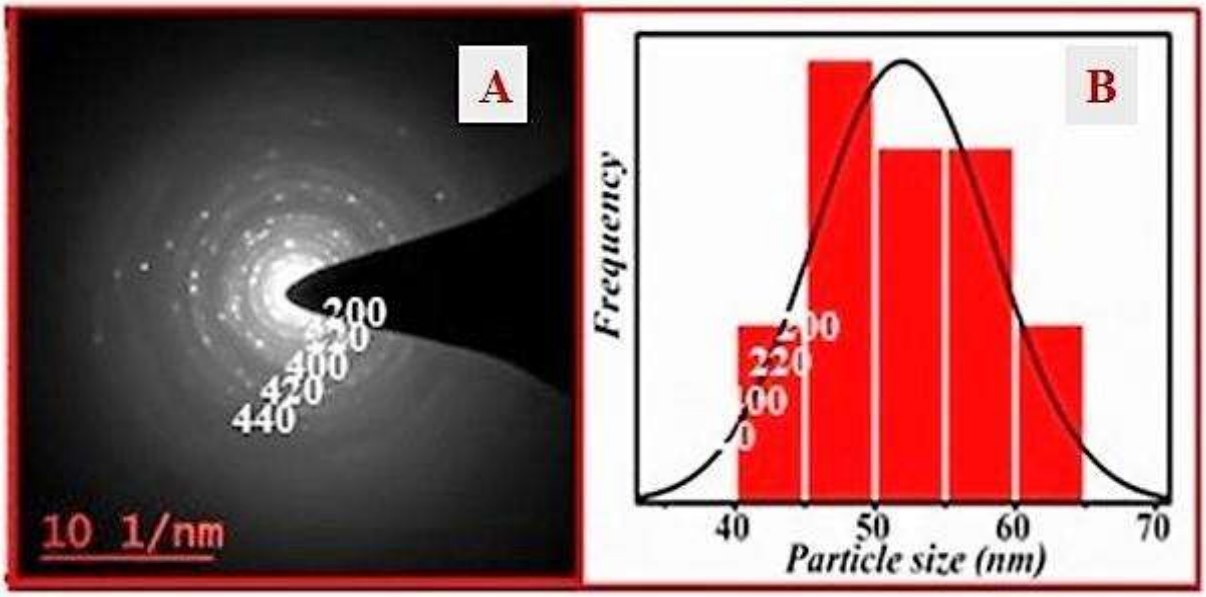

Figure 3.8: SAED pattern of PBN_1 (A), and bar histogram displaying the particle size distribution of corresponding nanoparticles (B).

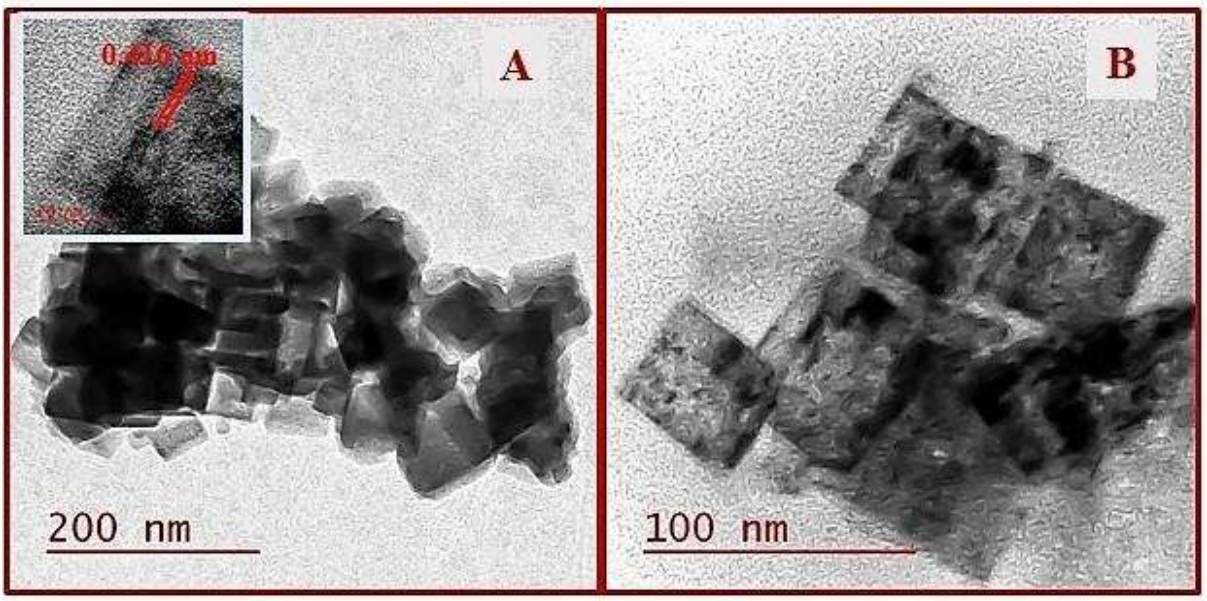

Figure 3.9: TEM images of PBN_2 (A,B), and the image shown in inset of (A) displayed lattice fringes of the corresponding nanoparticles.

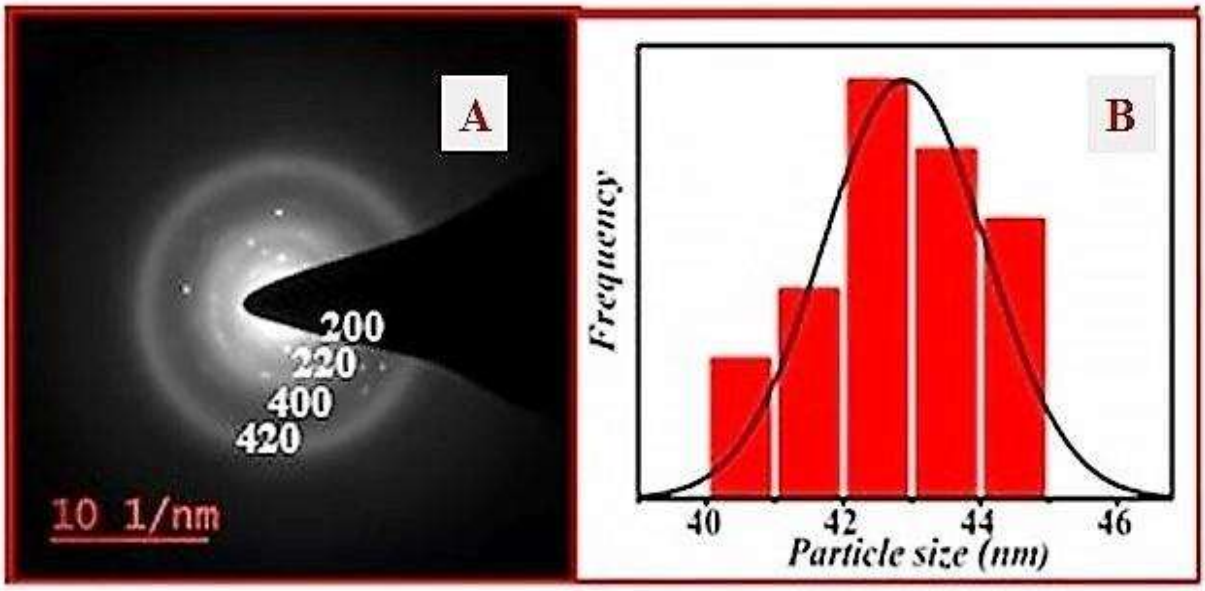

Figure 3.10: SAED pattern of PBN_2 (A), and bar histogram displaying the particle size distribution of corresponding nanoparticles (B).

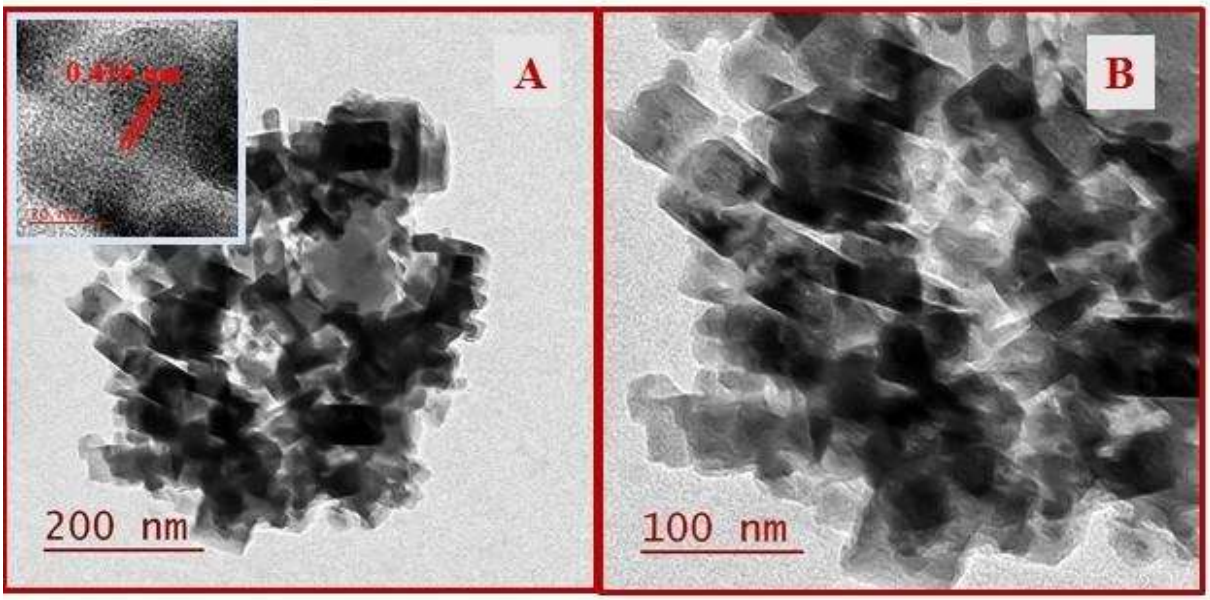

Figure 3.11: TEM images of PBN_3 (A,B), and the image shown in inset of (A) displayed lattice fringes of the corresponding nanoparticles.

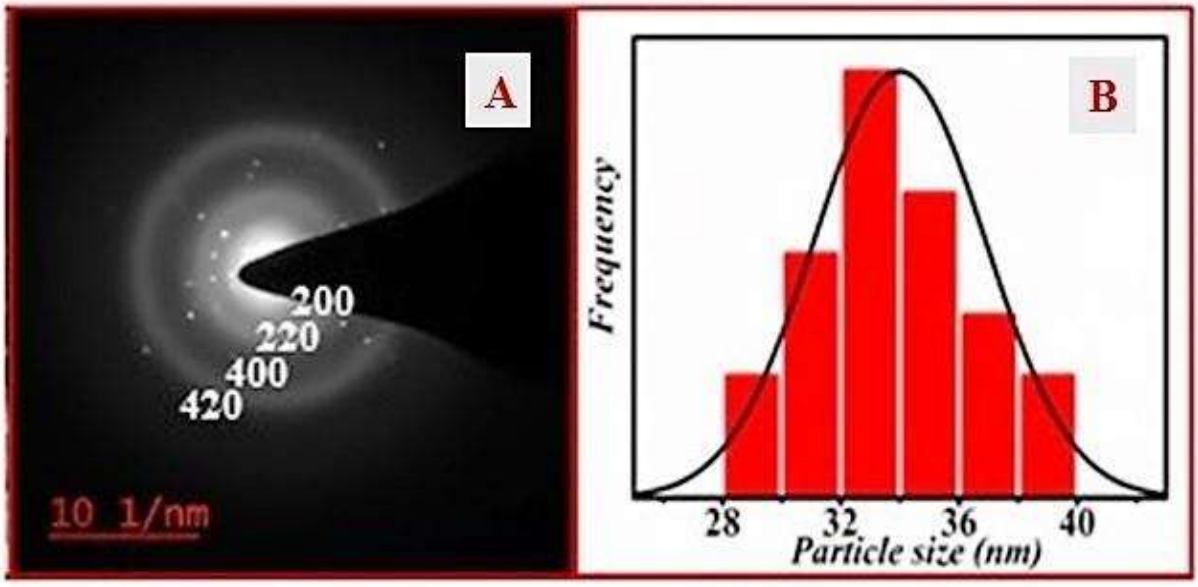

Figure 3.12: SAED pattern of PBN_3 (A), and bar histogram displaying the particle size distribution of corresponding nanoparticles (B).

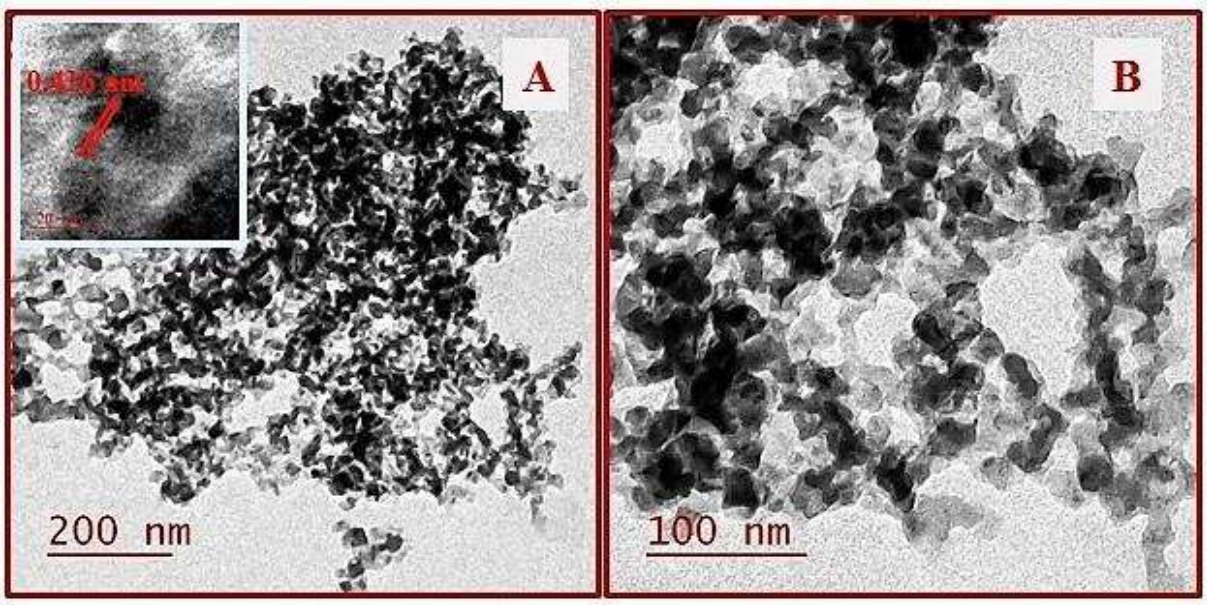

Figure 3.13: TEM images of PBN_4 (A,B), and the image shown in inset of (A) displayed lattice fringes of the corresponding nanoparticles.

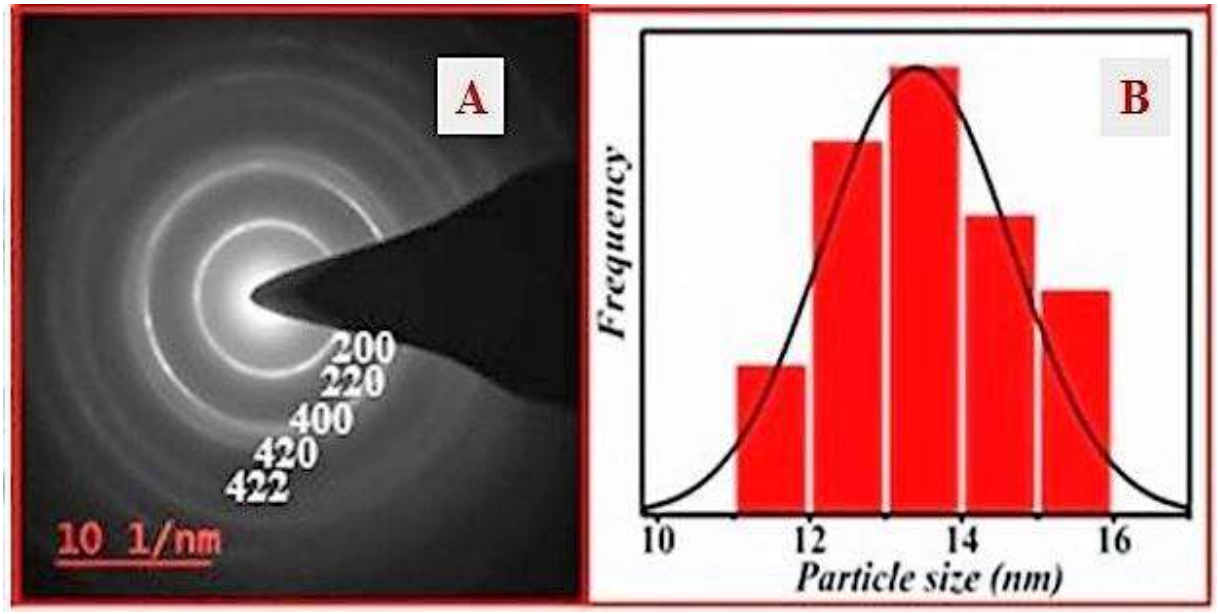

Figure 3.14: SAED pattern of PBN_4 (A), and bar histogram displaying the particle size distribution of corresponding nanoparticles (B).

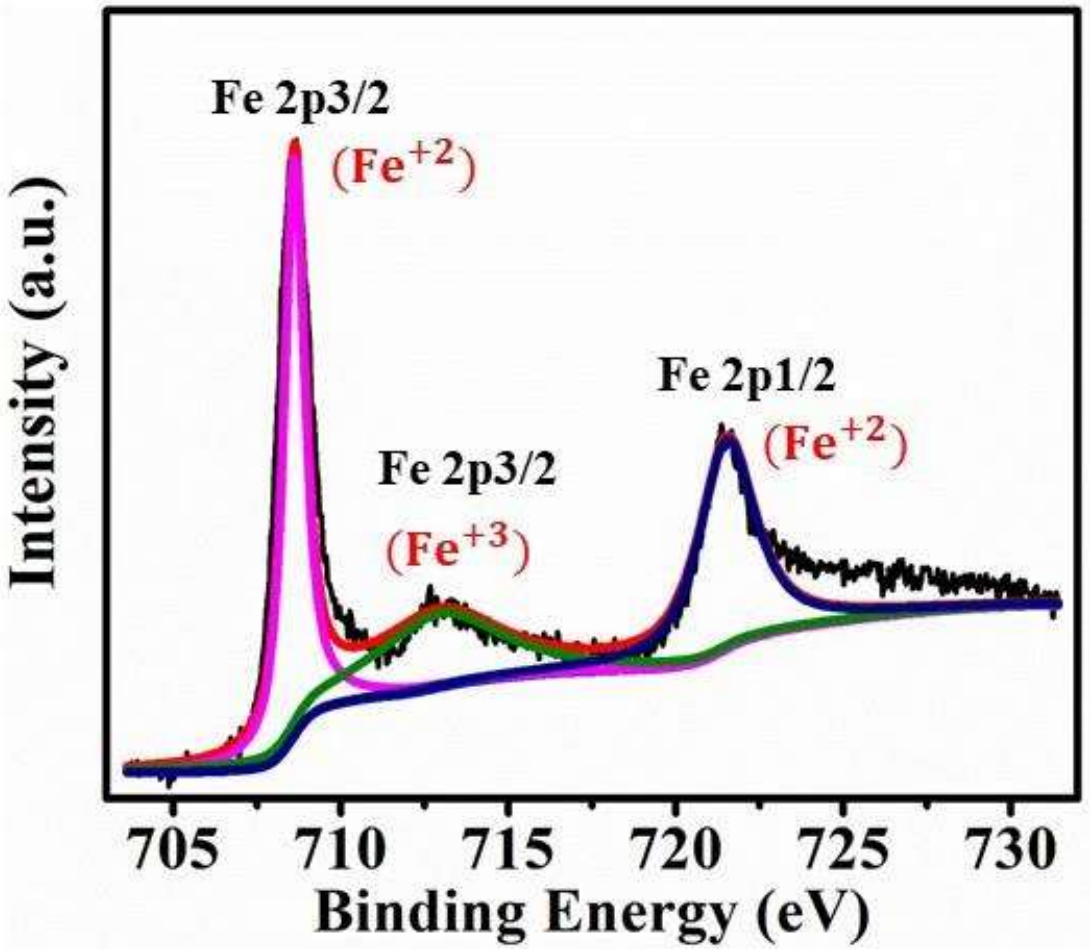

Figure 3.15: XPS analysis of PBN exhibiting presence of Fe^{+2} (BE of 721.87 eV and 708.64 eV) and Fe^{+3} (B.E. of 712.82 eV) chemical species in PBN.

---

of PB (Datta and Datta, 1990). Besides, the peak centred at B.E. of 712.82 eV clarified the featured Fe^{+3} species of PBN (Datta and Datta, 1990).

DLS characterization

The zeta potential of catalyst was measured as -2 mV, -7 mV, -13 mV and -20 mV (as displayed in Fig. 3.16) for PBN_1, PBN_2, PBN_3, and PBN_4 respectively corresponds to their negatively charged surface.

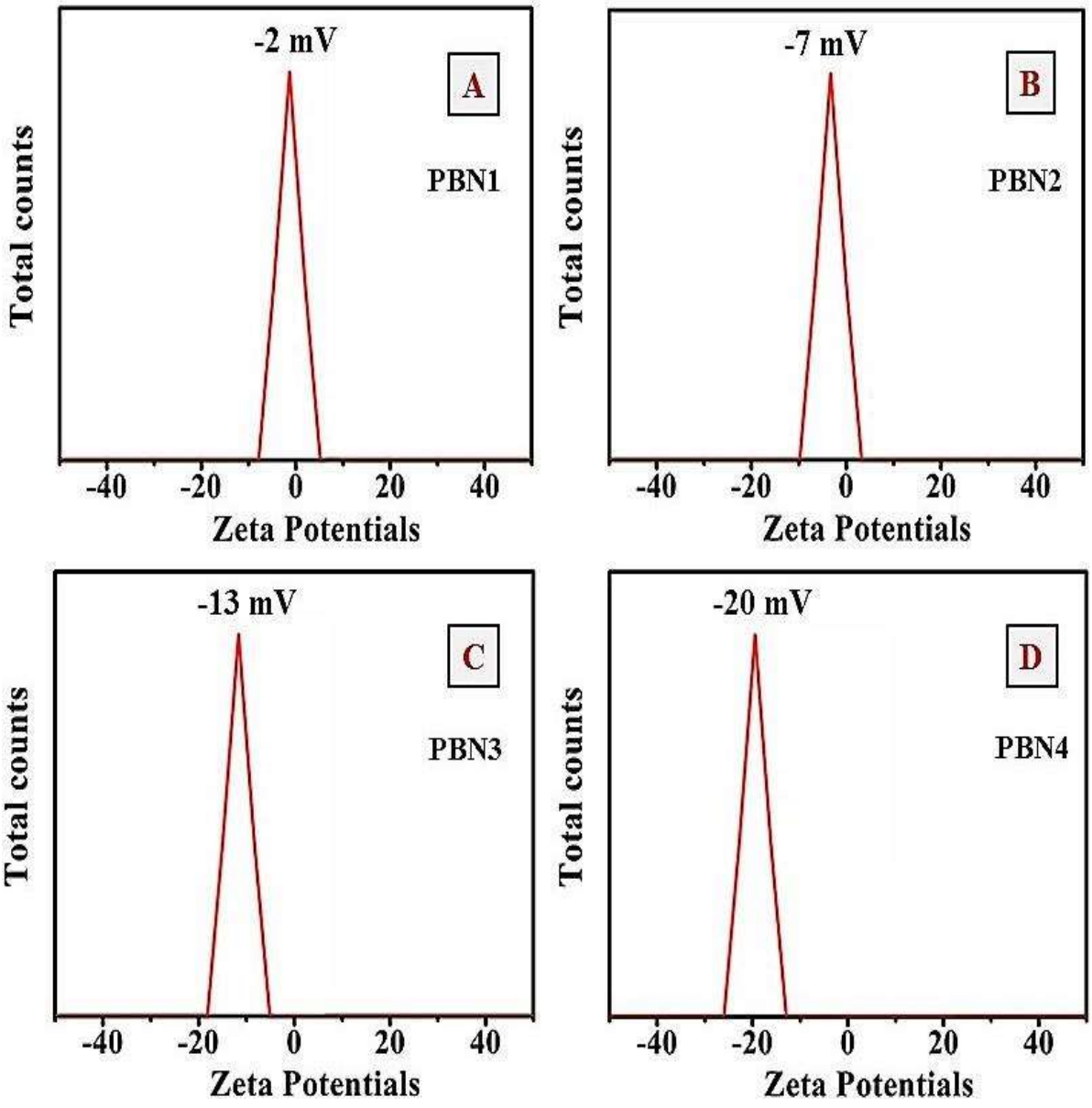

Figure 3.16: Measured zeta potentials of differently sized nanoparticles; PBN_1 (A), PBN_2 (B), PBN_3 (C), and PBN_4 (D) via DLS techniques.

3.3 RESULT AND DISCUSSION

3.3.1 Photowork for RhB degradation

The UV-vis spectroscopy actively displays a sharp and intense peak at 554 nm for RhB molecules. The degradation process of RhB using PBN and H_2O_2 was evaluated in absence and the presence of solar irradiation to justify the impact of solar energy. Fig. 3.17 (A) clearly reveals that only 7% dye has been degraded under normal ambience (RT) and experimental conditions. The effect of temperature has also been examined under dark condition to understand the variation in degradation rate. The results (Fig. 3.17 (B)) justify only 13% degradation at 343K while keeping other conditions constant. Subsequently, the effect of UV lamp was further evaluated to verify the significance of solar radiation on the degradation process as shown in Fig. 3.17 (C). Nearly 22% dye degradation was observed. under UV lamp exposure indicating the significance of solar radiation on degradation process. Accordingly, the dye degradation was studied under solar radiation while keeping other condition constant as shown in Fig. 3.17 (D). Consequently complete degradation (100%) of dye has been achieved, justifying the active role of PBN under solar radiation as given in table 3.1.

Further to go into more insight to understand the influence of all reacting components on RhB photodegradation, the experiment was carried out under solar radiation in different condition; (i) in absence of PBN as well as H_2O_2 (Fig. 3.18 A), (ii) only H_2O_2 (Fig. 3.18 B), (iii) only PBN (Fig. 3.18 C), and (iv) PBN-H_2O_2 (Fig. 3.18 D). The efficiency of photocatalytic degradation of RhB has been estimated under these conditions and results are recorded in table 3.1. The results indicate 3%, 17%, 23% and 100% degradation of RhB under four different conditions (Fig. 3.19 and Table 3.1), justifying the role of both H_2O_2 and PBN on degradation process. Accordingly, the activity of PBN in the presence of H_2O_2 was evaluated to understand the mechanistic approach on photodegradation process. The reactive $OH^{\bullet}$ generated throughout the photolysis of H_2O_2 was supposed to undergo dimerization as later act as a scavenger for in-situ generated free radicals. On contrary, when mixture was irradiated with addition of H_2O_2 and PBN at pH-7 under solar light, it shows almost complete degradation of dye (Fig. 3.19). A modest decrease in absorbance maxima at 680nm for PBN and an exalted

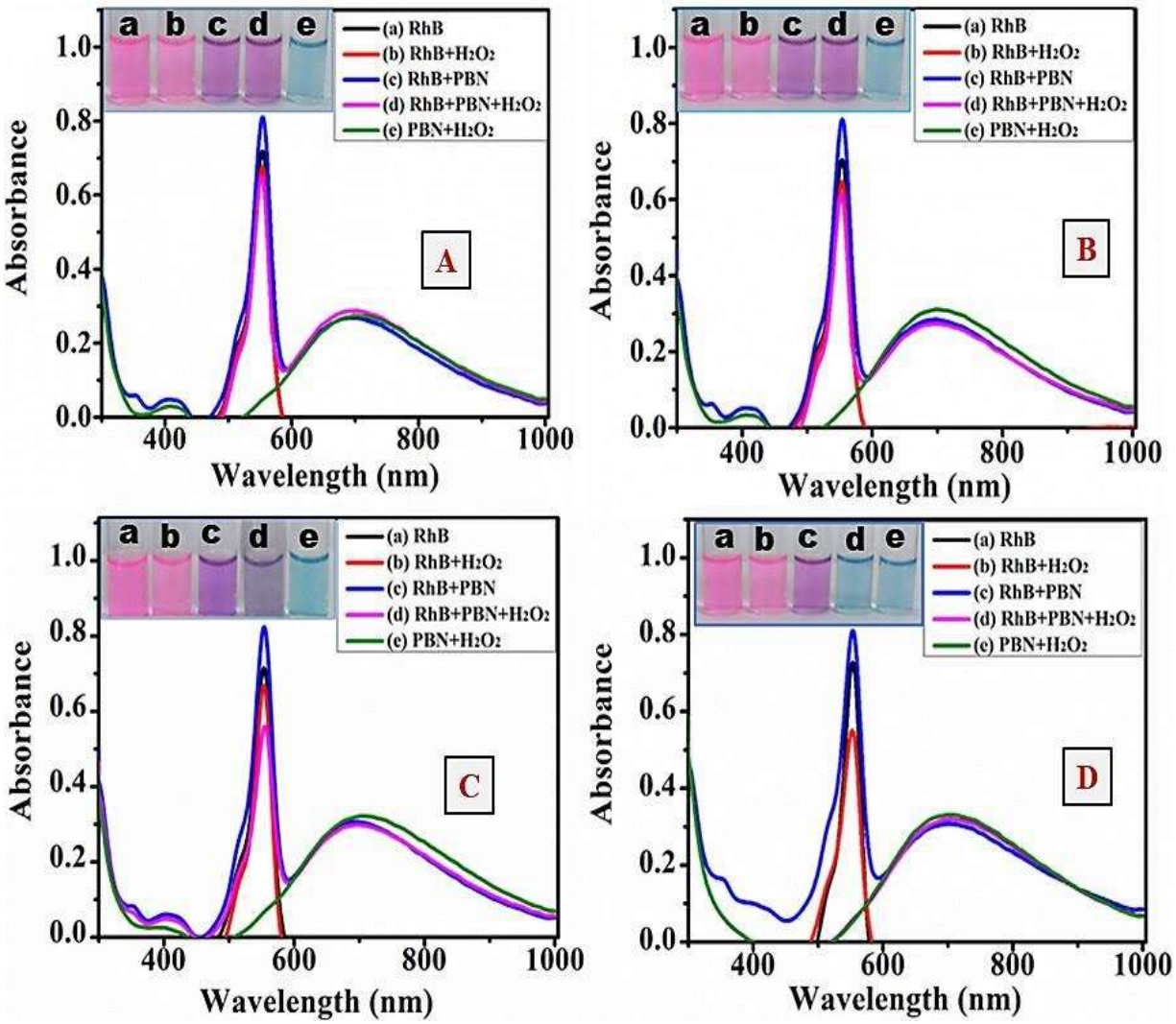

Figure 3.17: UV-Vis spectrum of aqueous RhB solution (10 ppm) degradation using PBN/H_2O_2 (0.5 mM/10 mM) in different condition; RT (A), oven (B), UV-lamp (C), and solar light (D).

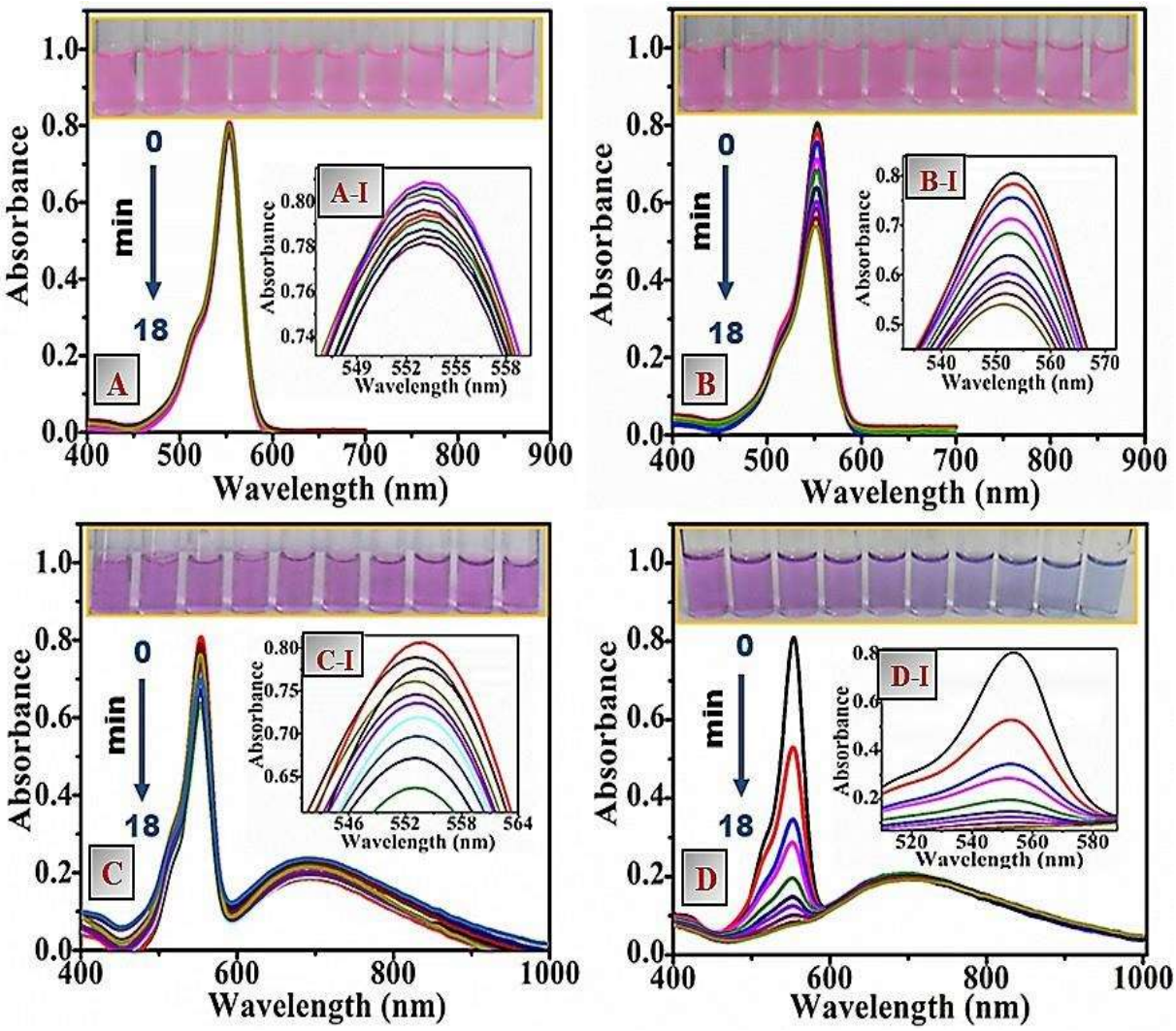

Figure 3.18: Recorded UV-Vis spectrum (with magnified view) of RhB during photodegradation under solar light in different systems; RhB (10 ppm) (A, A-I), RhB (10 ppm)-H_2O_2 (1.0 mM) (B, B-I), RhB (10 ppm)-PBN (0.5 mM) (C, C-I), and RhB (10 ppm)-H_2O_2 (10 mM)-PBN (0.5 mM) (D, D-I).

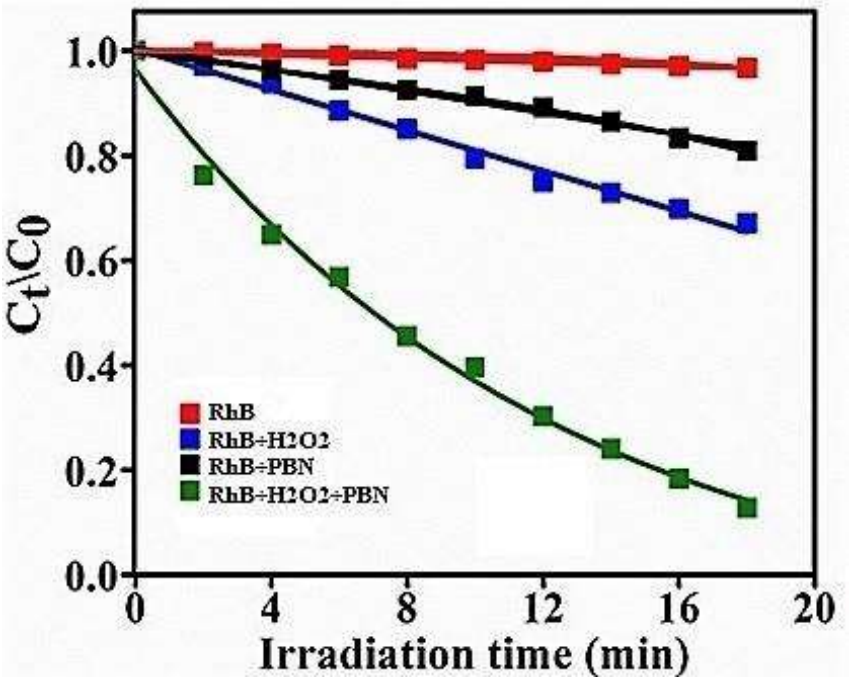

Figure 3.19: Effect of the irradiation time on photocatalytic degradation process recoded in different reactant conditions.

peak at 554 nm for RhB estimates specific interaction between catalyst and target molecule. H_2O_2 addition initiates consecutive decrease in absorbance peak at 554 nm as a resultant of RhB degradation. Further, absence of absorbance at 554 nm and a broad peak at 680 nm shows the complete degradation of dye and unaffected recycled photo-Fenton catalyst. Again, the experiment was repeated while varying essential parameters, such as catalyst amount, effect of catalyst size and the concentration of H_2O_2 to understand their substantial impact over photo-catalytic degradation of RhB.

Effect of Catalyst concentration on RhB degradation

The influential impact of the catalyst over RhB photodegradation was evaluated by implementing several experiments, where PBN amount was varied (0.5 - 1.5 mM) while keeping RhB (10 ppm) and H_2O_2 (10 mM) constant. The outcome of experiments is displayed through absorption spectra as shown in Fig. 3.20(A,B,C). The photocatalytic rate was expected to increase enormously with high dosages of catalyst as were presumed to produce more hydroxyl radical. However, a slight rise in performance was observed during RhB photodegradation as can be seen in Fig. 3.20(A,B,C). This might be attributed due

Table 3.1: Comparative study of RhB degradation under different conditions.

System	Reaction condition	Time of exposure	%Degradation
RhB+PBN+H_2O_2	RT	18 min	7%
RhB+PBN+H_2O_2	343 K	18 min	13%
RhB+PBN+H_2O_2	UV Lamp	18 min	22%
RhB	Solar light	18 min	3%
RhB+H_2O_2	Solar light	18 min	17%
RhB+PBN	Solar light	18 min	23%
RhB+PBN+H_2O_2	Solar light	18 min	100%

to high coloured reaction environment that makes solution turbid and causes shelteringof light and similarly interrupt the generated hydroxyl radical to reach on the surface of the RhB molecule (Cui et al., 2014).

Effect of H_2O_2 concentration variation on degradation

Effect of the initial concentration of H_2O_2 on the photodegradation of RhB was also investigated. As the number of photocatalytic experiments was done via varying H_2O_2 (10mM, 20 mM, and 30 mM) with a fixed catalyst (0.5 mM) and RhB (10 ppm) concentrationas displays in Fig. 3.20(D,E,F). Addition of H_2O_2 along with PBN in RhB solution began to an apparent reduction in absorbance at 554 and tended to increase the degradation rate progressively with increase in their concentrations as shown in Fig. 3.20(D, E, F). However, the degradation rate was found more progressive with H_2O_2 high amount as compared to a rise in catalyst concentration. A prominent rise in rate observed was elevated by an attack of peroxide to central in the RhB to cause breaking of C−C bond (Mehrdad and Hashemzadeh, 2009). The effect of irradiation time on photocatalysis was performed using different amount of catalyst (0.5 mM, 1.0 mM, 1.5 mM) as well as H_2O_2 (10 mM, 20 mM, 30 mM) as displayed in Fig. 3.21A and Fig. 3.21B respectively, evident to the rise in degradation rate respective of their content. So it simplifies that optimum concentration of photo-Fenton catalyst (PBN) and H_2O_2 was required for effective photodegradation process.

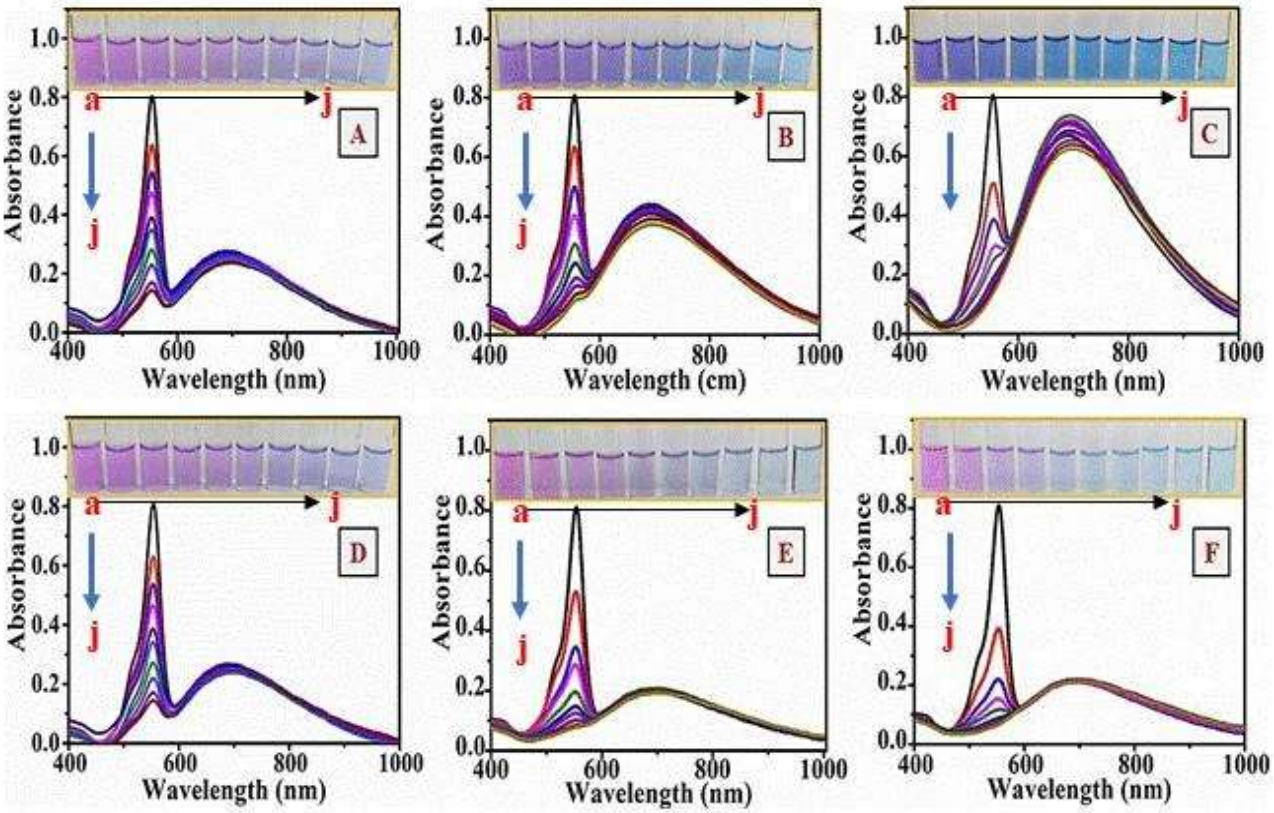

Figure 3.20: Effect of PBN concentration variation (A = 0.5 mM, B = 1.0 mM, C = 1.5 mM) with continual concentration of H_2O_2 (10 mM), and effect of H_2O_2 concentration variation (D = 10 mM, E = 20 mM, F = 30 mM) with continual concentration of PBN (0.5 mM) on solar light assisted photo-Fenton degradation of RhB (10ppm) in RhB-PBN-H_2O_2 system as recorded in UV-Vis spectrum.

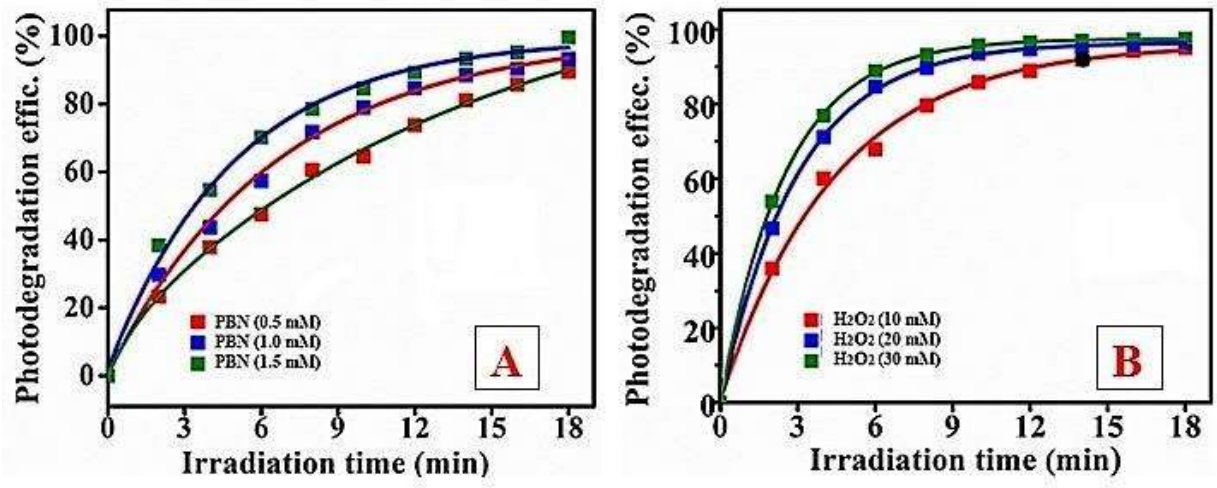

Figure 3.21: Concentration variation influence of catalyst PBN (0.5 mM-1.5 mM) with continual H_2O_2 (10 mM) and RhB (10 ppm) (A), and H_2O_2 (10 mM-30 mM) with con- tinual PBN (0.5 mM) and RhB (10 ppm) (B) on the irradiation time of photocatalytic degradation process in RhB-H_2O_2-PBN system.

The photo-Fenton process encompassing, PBN and H_2O_2 reacts to generate enormously active hydroxyl radicals, which is responsible for the RhB degradation.

$$OH^{\bullet} + RhB \rightarrow products$$

Catalyst size effect on photodegradation process

Further, in order to evaluate the impact of nano-size over RhB degradation, the photo-Fenton process was performed with catalysts such as; PBN_1 (Fig. 3.22A), PBN_2 (Fig. 3.22B), PBN_3 (Fig. 3.22C) and PBN_4 (Fig. 3.22D) under similar condition. The spectral changes at 554 nm for dye was noticeably decreased along with size during a reaction. Meanwhile, the changes are very rapid for smaller one PBN_4 (13 nm). Allowed size effect over dye degradation was attributed due to availability of spare active molecule of PBN, that provides an additional surface to grab more RhB molecules on the surface and to process their degradation rate employing photo-Fenton reaction. Small particle size was supposed to reduce the diffusion path length for the Fenton-process generated hydroxyl radical. The hydroxyl radical effectively produced, reacted and hence shows higher photocatalytic activity.

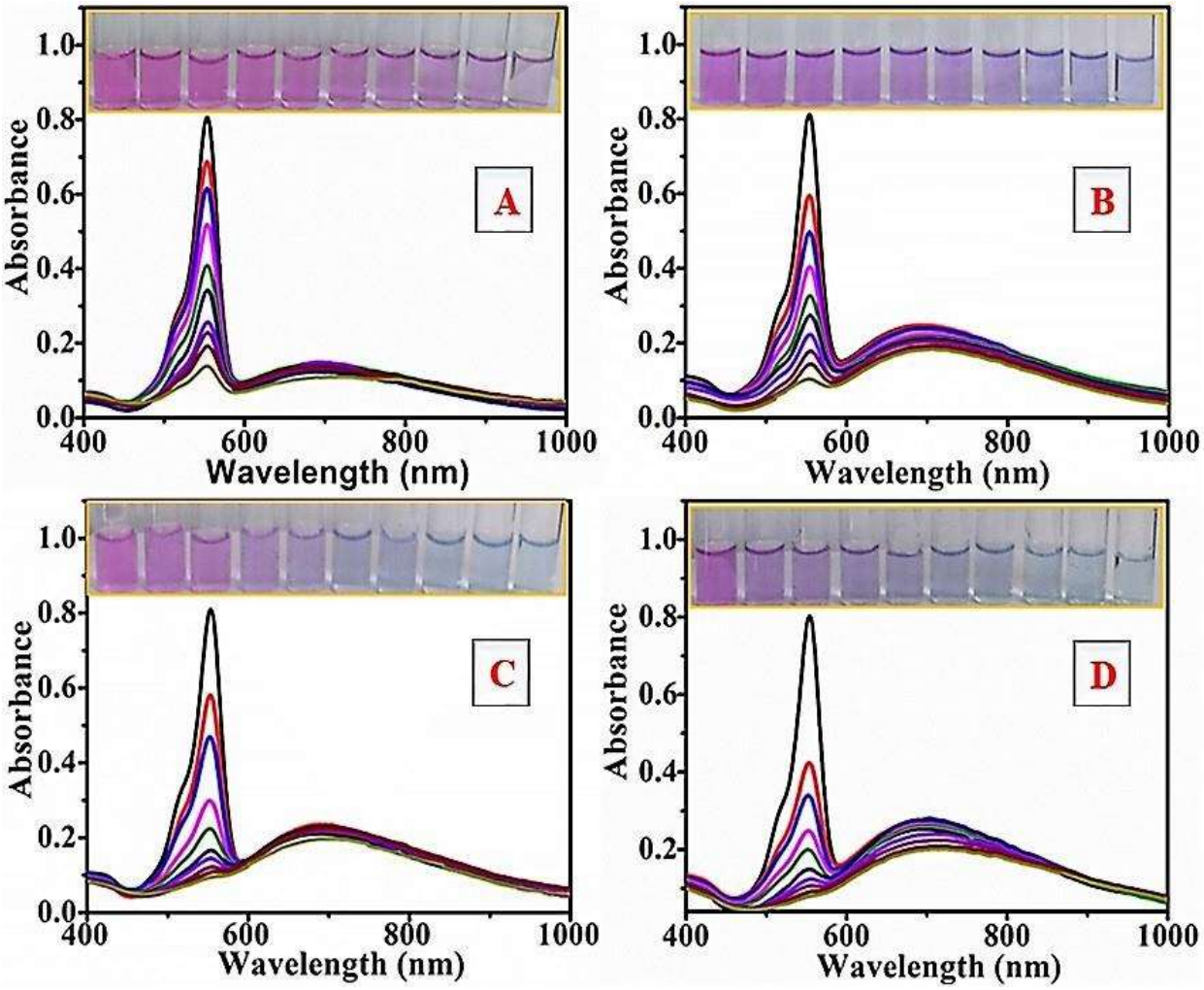

Figure 3.22: Size influence of photo-Fenton catalyst PBN_1 (A), PBN_2 (B), PBN_3 (C), and PBN_4 (D) over RhB (10ppm) degradation with H_2O_2 (10 mM) in RhB-H_2O_2-PBN system.

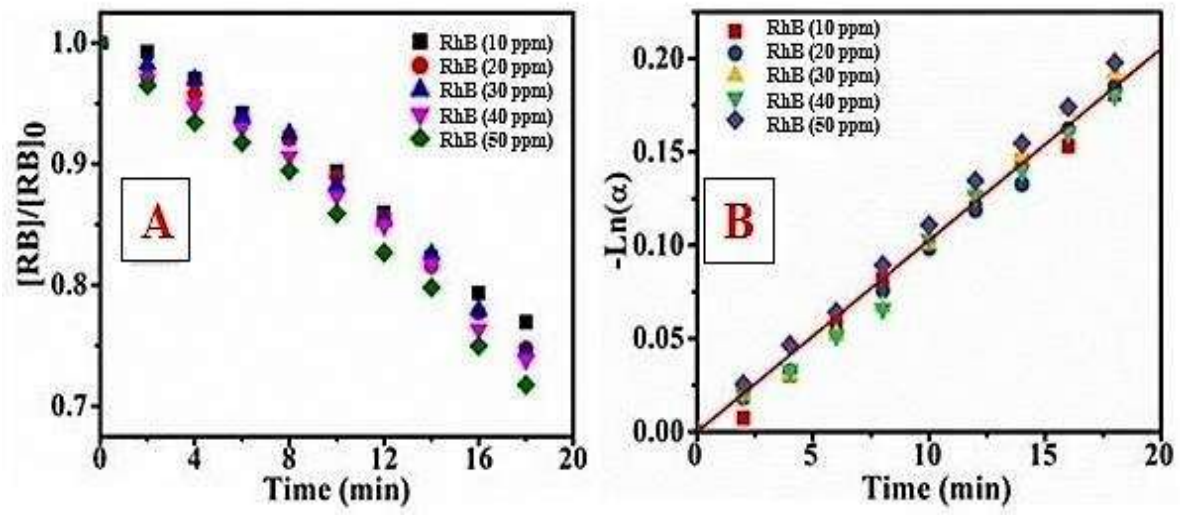

Figure 3.23: Relationship between unreacted fraction of RhB of different concentration (10-50 ppm) vs. irradiation time using constant H_2O_2 (10 mM) (A). Linear relation between Ln(α) vs. degradation time for different concentration of RhB with H_2O_2 (B).

3.3.2 Kinetic study of photo-Fenton degradation process

Further, some more experiments were performed sequentially at pH-7 to study the kinetics of photodegradation process to evaluate the rate constant and order with respect to H_2O_2 and PBN. The particular trials are reported here as follows.

Different concentration of RhB

Initially, the experiment was carried out by varying RhB concentration (10-50 ppm) with continual H_2O_2 concentration (10 mM) under solar light. The RhB shows consecutive change at absorption maxima (λmax-554 nm) respective of their degradation (Fig. 3.23 A). The unreacted fraction (α = C/C_o) of RhB was evaluated by using a calibration curve and Beer's law (A= ξbc). The linear relationship between ln(α) and degradation time (t) shows that the degradation of RhB is independent of the initial concentration of time and it follows first-order kinetic. The rate equation for the degradation of RhB in the presence of H_2O_2 is:

$$d[RB]/dt = -k[H_2O_2]^m\ [RB] = -k^t\ [RB]$$

$$\ln\ [RB]/[RB]_o = \ln(\alpha) = -k^t t$$

The relationship between ln(α) and degradation time (t) is linear as shown in Fig. 3.23 B. The apparent rate constant $k^t = k[H_2O_2]^m$ was attained 2.82±0.010 × 10^{-4} min^{-1} from the slope of ln(α) vs. degradation time (t) for the RhB degradation in the presence of H_2O_2 (Fig. 3.23B).

Effect of H_2O_2 concentration

Further, to study the effect of H_2O_2 concentration on the photocatalytic degradation of RhB (10 ppm), the experiment was carried out only with various concentrations of H_2O_2 i.e.:10 mM, 20 mM, 30 mM with constant RhB in absence of PBN and allow itto irradiated under solar light. The unreacted fractions of RhB (with respect to various concentration of H_2O_2) after degradation were calculated from the absorption spectra by using a calibration curve and Beer's law (A= ξbc). The outcome of this experiment was revealed in Fig. 3.24A. The linear relationship between ln(k) and degradation time (t), as displayed in Fig. 3.24B, indicated the impact of H_2O_2 on the RhB degradation rate. The apparent rate constants; 0.01517 ±.00069, 0.01903 ±0.00039, and 0.02360±0.00052 min^{-1} were obtained from the slopes procured at different concentrations i.e; 10 mM, 20 mM, and 30 mM of H_2O_2, respectively. Further, the rate constant and order of reaction was derived from the intercept and slope of ln(k) vs. ln H_2O_2 from the Fig. 3.24C. While considering the attained rate constant and order concerning H_2O_2, the rate equation derived for the degradation of RhB is:

$$d[RB]/dt = -0.075[H_2O_2]^{0.40}\,[RB]$$

Kinetics study after the addition of Catalyst

After most, the photocatalytic degradation of RhB was performed with constant H_2O_2 (10 mM) and RhB (10 ppm) concentration while using PBN of different amount (0.5 mM, 1.0 mM, 1.5 mM). The unreacted fractions of RhB after degradation were calculated from the absorption spectra by using a calibration curve and Beer's law (A=ξbc) as displayed in Fig. 3.25A. The linear relationship between ln(α) and degradation time (t) suggest that RhB degradation follows first-order kinetics. The rate equation for RhB degradation in the presence of the different amount of catalyst can be written as:

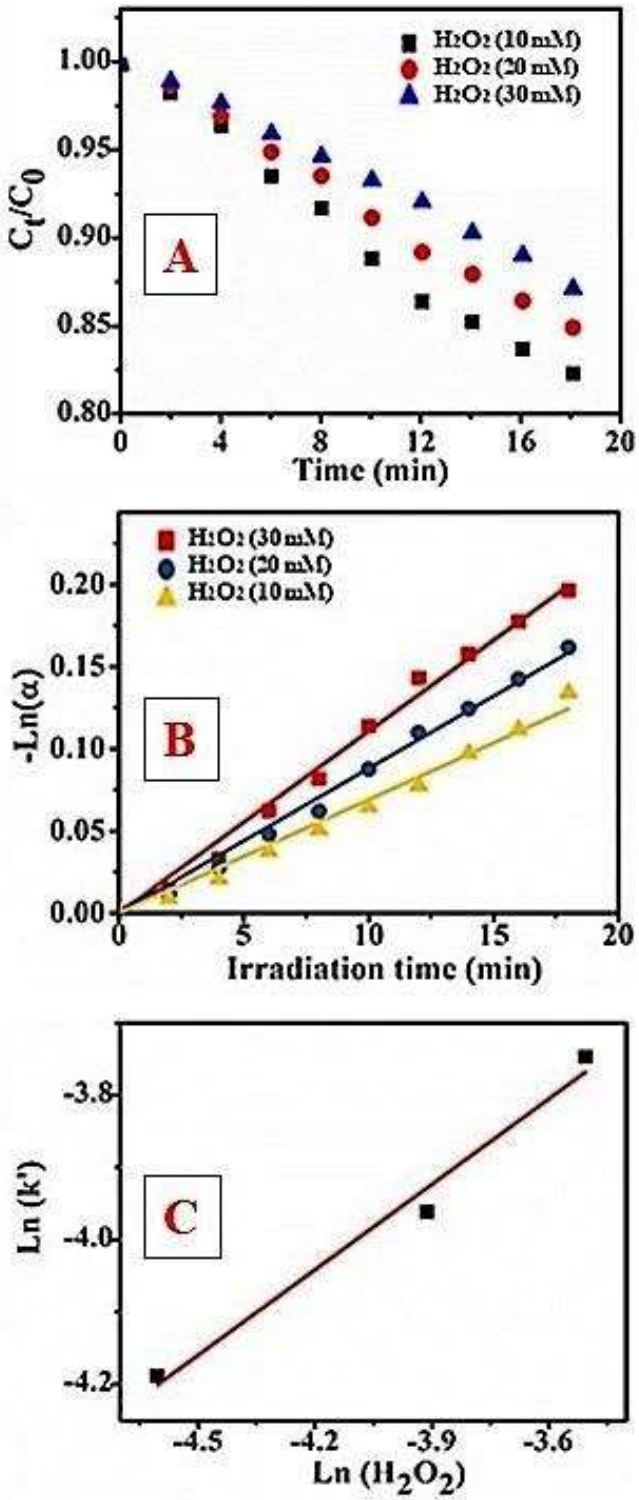

Figure 3.24: Relationship between unreacted fraction of RhB (10 ppm) vs. irradiation time with varying H_2O_2 (10mM-30mM) concentrations (A). Linear relationship between Ln(α) vs. degradation time for different concentration of H_2O_2 (B). And plot of Ln (k) vs. Ln (H_2O_2) for RhB photodegradation (C).

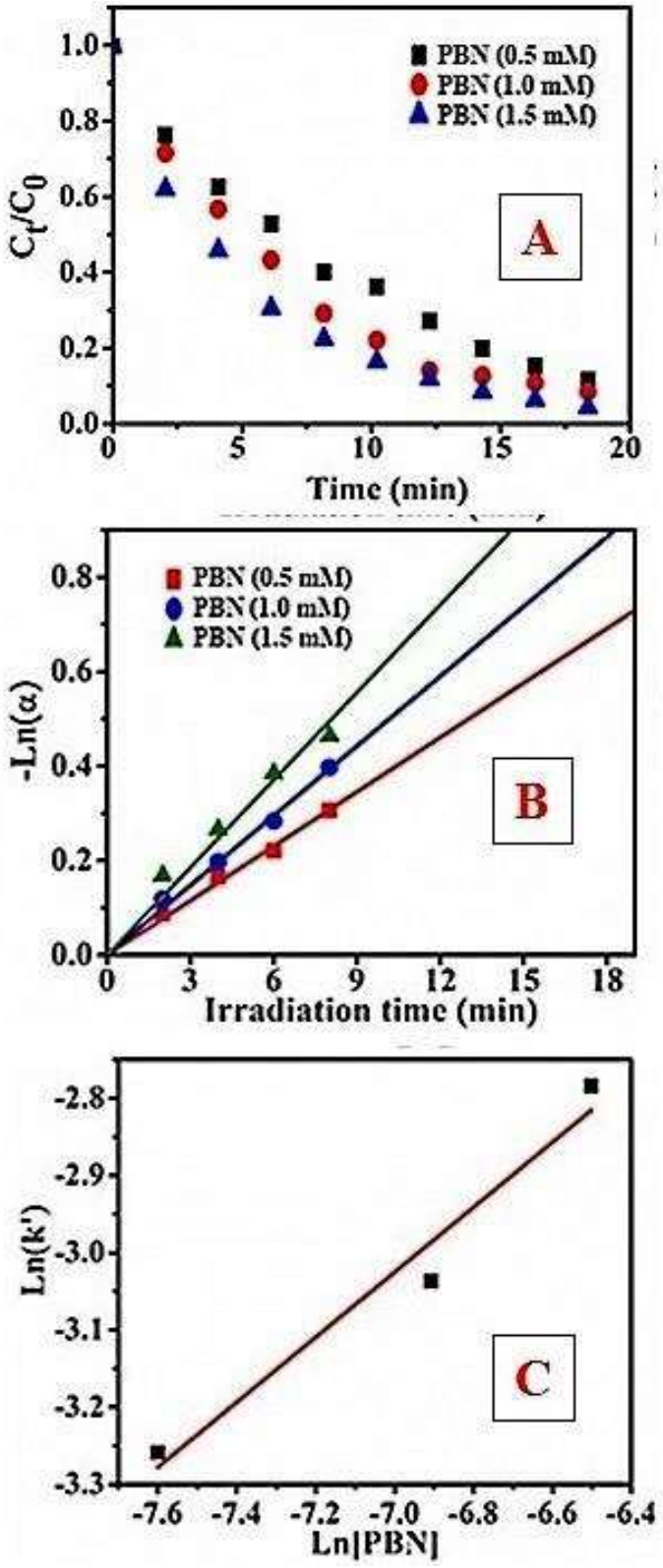

Figure 3.25: Relationship between unreacted fraction of RhB (10 ppm) vs. irradiation time using constant H_2O_2 (10 mM) and different catalyst (0.5 mM-1.5 mM) concentrations(A). Linear relationship between ln(α) vs. degradation time in different concentration of PBN (0.5 mM-1.5 mM) with constant H_2O_2 (10 mM) and RhB (10 ppm) (B). Plot of Ln (k) vs. Ln (PBN) for RhB photodegradation (C).

$$d[RB]/dt = -k[H_2O_2]^n [FeO]^m [RB] = -k'' [FeO]^m[RB] = -k^t[RB]$$

$$\ln [RB]/[RB]_o = \ln(\alpha) = -k^t t$$

Where, $k^t = k'' [FeO]^m = k[H_2O_2]^n [FeO]^m$. The apparent rate constants are 0.03842± 0.0015, 0.04721±0.0019, and 0.06189±0.0037 for PBN (0.5 mM), PBN (1.0 mM) and PBN (1.5 mM) respectively, as shown in Fig. 3.25B. The subsequent apparent rate constant obtained from the slopes of Fig. 3.25B, reveal concentration-dependent rate. Consequently degradation process became more fastest as catalyst dosage increment to a specific limit. The order respective of PBN amount was derived from the plot of ln(k) vs. ln(PBN) from Fig. 3.25C. So, the rate equation of the RhB degradation in the presence of H_2O_2 and PBN as follows.

$$d[RB]/dt = -0.935[FeO]^{0.42} [RB]$$

It is noticeable that the RhB photodegradation follows pseudo-first order kinetics. A linear relationship between ln (C_t/C_o) and irradiation time (t) shows a very high rate constant (0.935 min^{-1}) which is many more fold times greater than the previous reports for the same. Besides, the kinetics carried out with photo-Fenton process encompasses PBN_4 along with H_2O_2 achieved 13 times higher rate than the photodegradation processed with H_2O_2 individually. The kinetic rate constant values obtained for all size of nanoparticles such as PBN_1, PBN_2, PBN_3 and PBN_4, listed in Table 3.2 displays that performance of smallest sized (PBN_4) is higher than the larger one (PBN_1). Besides, PBN−H_2O_2 combination remarkably decreased the half-life time required for 50% degradation of the initial concentration of RhB, in particular, those supported with PBN_4.

Table 3.2: Kinetic analysis of different degradation system

Degradation System	Kinetic rate constant (min-1)	Half-life (min)	R-squared (R^2)
H_2O_2	0.003934 ± 0.00025	9.20	0.96
$PBN_1+H_2O_2$	0.8621 ± 0.0631	0.80	0.99
$PBN_2+H_2O_2$	0.8873 ± 0.0154	0.78	0.98
$PBN_3+H_2O_2$	0.9028 ± 0.019	0.76	0.96
$PBN_4+H_2O_2$	0.9353 ± 0.0356	0.75	0.99

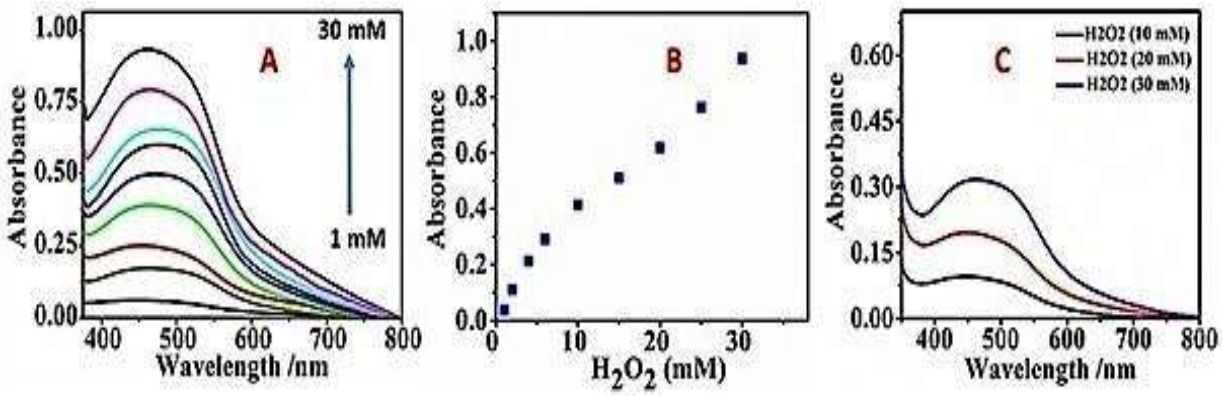

Figure 3.26: Recorded absorbance maxima (λmax = 480 nm) as a function of H_2O_2 (1mM-30mM) concentrations correspond to the oxidized product of o-dianisidine dye (25 μM) in the presence of PBN (1 mM) (A). Calibration curve displaying H_2O_2 concentration (1 mM-30 mM) dependent change in the absorbance maxima at 480 nm (B). And change in absorption for o-dianisidine-PBN-H_2O_2 complex with respect to residual amount of H_2O_2 (10 mM, 20 mM, 30 mM) after photodegradation process (C).

Quantification of residual H_2O_2, after photodegradation, were estimated via simple colorimetric method. The method was based on H_2O_2 interaction with peroxidase chromogenic substrate o-dianisidine in the presence of PBN (artificial peroxidase enzyme) which produced a stable orange-red product having absorbance maxima at 480 nm. Accordingly, two distinct experiment was performed; (I) In the first set of analysis, different concentration of H_2O_2 (1mM-30 mM) was added with fixed o-dianisidine (25 μM), and PBN (1 mM) in 1.5 ml of Milli-Q water and their absorption spectra was recorded that revealed a peak at 480 nm.

Change in absorbance maxima were recorded (480 nm) as a function of varying concentration of H_2O_2 (1-30mM) at room temperature correspond to the oxidized product of o-dianisidine (25 μM) in the presence of PBN (1 mM) (Fig. 3.26A). The calibration curve obtained displaying change in absorbance maxima at 480 nm as the function of H_2O_2 concentration (1 mM-30 mM) variation (Fig. 3.26B). In second set of experiment, further 10 mM, 20 mM, and 30 mM concentration of H_2O_2 were added in reaction system (2 ml of milli-Q water) with catalyst and RhB (10ppm) and allowed it to irradiate under solar light for photo-Fenton process. After completion of dye degradation, 1.5 ml of each supernatant (after centrifugation) were pipette out and added subsequently with o-dianisidine (25 μM)

and PBN (1 mM). The recorded absorption maxima, correspond to o-dianisidine-H_2O_2 complex formation in presence of PBN, indicates the residual amount of the H_2O_2 (10 mM, 20 mM, 30 mM) and anticipated consumed amount of H_2O_2 throughout the RhB photodegradation process (Fig. 3.26C and Table 3.3).

Table 3.3: Data listed here displaying the amount of H_2O_2 concentration used in degradation process based on the coloured complex formation.

System	Absorbance (A_0)	Absorbance (A_t)	Amount of H_2O_2 (%)
H_2O_2 (30 mM)	0.96	0.33	65.20
H_2O_2 (20 mM)	0.61	0.19	68.55
H_2O_2 (10 mM)	0.44	0.09	79.02

3.3.3 Rhodamine B photodegradation

RhB primarily exists in two forms in water, i.e., the zwitter ionic ($RhB^{\pm}$) in basic range and cationic form (RhB^{+}) in acidic medium. Generally, it was found to be very firm; however, the addition of the photo-Fenton complex quickly initiated RhB degradation and suggested to involve three phases; A) N-deethylation of RhB. B) cleavage of chromophore ring. and C) mineralization of the dye into CO_2 and H_2O. The impact of pH on the rate of photodegradation process was also interpreted. Several experiments were carried out at a fixed concentration of the dye (10 ppm) in various pH, ranging from 2-12. Changing in medium pH expressively affects the rate by altering charge on the pollutants and consequently influencing the adsorption of dye, as the number of adsorption sites on the catalyst increased.

As the degradation proceeded, the hypochromic shift due to succeeding de-ethylationfrom the aromatic ring (Sun et al., 2017) was more profound with an additional evident blue shift (λmax-537nm) in acidic medium (Fig. 3.27A). While in alkaline medium the characteristics peak of the RhB shows an unexpectedly hypochromic shift in the absorption maxima (λmax-554nm) as a result of chromophore cleavage (Fig. 3.27B). The characteristic absorption peak occurred at a lower wavelength revealed the auxochromic property of the N-ethyl group (Chen et al., 2002). Most of the N-deethylation processes

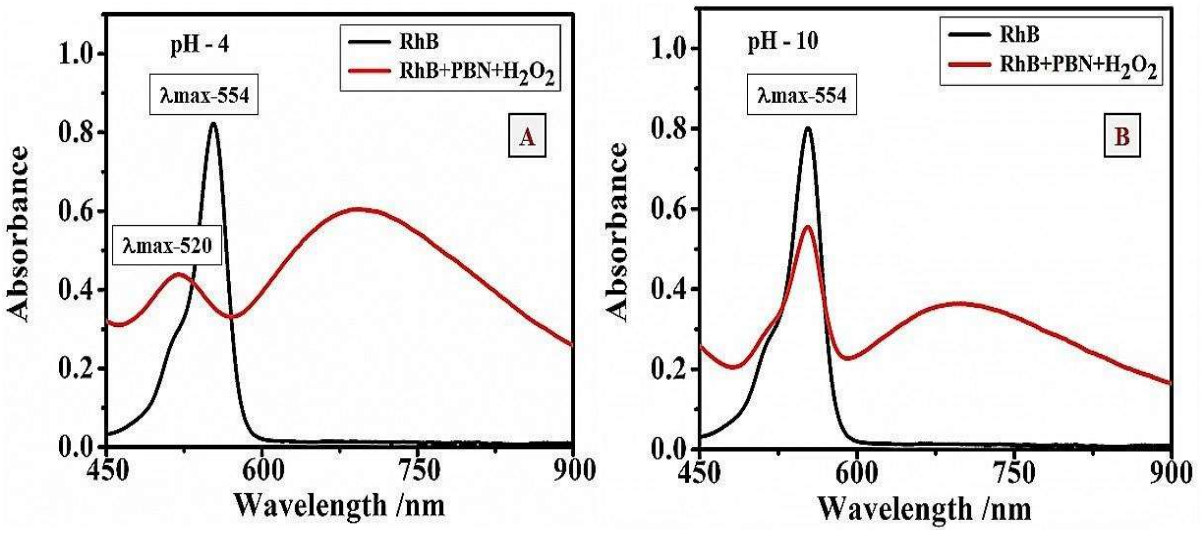

Figure 3.27: Hypsochromic (blue shift) and hypochromic shift in absorption maxima peak of RhB during the photodegradation process in acidic (A), and alkaline (B) medium.

---

are accountable by nitrogen-centered radicals, while ring cleavage is by carbon-centered radical formation. The effect of RhB degradation over PBN has also been evaluated based on zeta potential measurement (Fig. 3.16), which reveals the negative surface of the catalyst and appeals to the positively charged ethylamine to preferential adsorbed on the surface of it through nitrogen-center. It was observed that the nanoparticles remain unaffected during the reaction. It is relevant to note that the rate of photodegradation process was found to influence by medium and shows higher efficiency in the acidic reaction condition due to the following reasons; (i) sequential removal of ethyl moiety would transfer whole electron density and supposed to generate positive centers (Rh^{+}) (Yu et al., 2009). (ii) in acidic medium cationic form of dye (RhB^{+}) easily get attracted to the negatively charged surface of PBN (ζ = -2 to -20 mV). (iii) the rate of hydroxyl radical formation was very high as per photo-Fenton reaction supremely favored in acidic medium (Barbusiński, 2009).Conversely, photodegradation implemented at higher pH corresponds to the low rate, as both diethyls connected in the dimeric form of RhB might sterically hinder active radical attack.

The photodegraded end products in acidic (Fig. 3.28B) and alkaline medium (Fig. 3.28C) were detected and identified by LC- MS analysis as depicted in Fig. 3.28. A sharpand intense peak at m/z of 443 correspond to the LC-MS spectra of RhB (Fig. 3.28A).

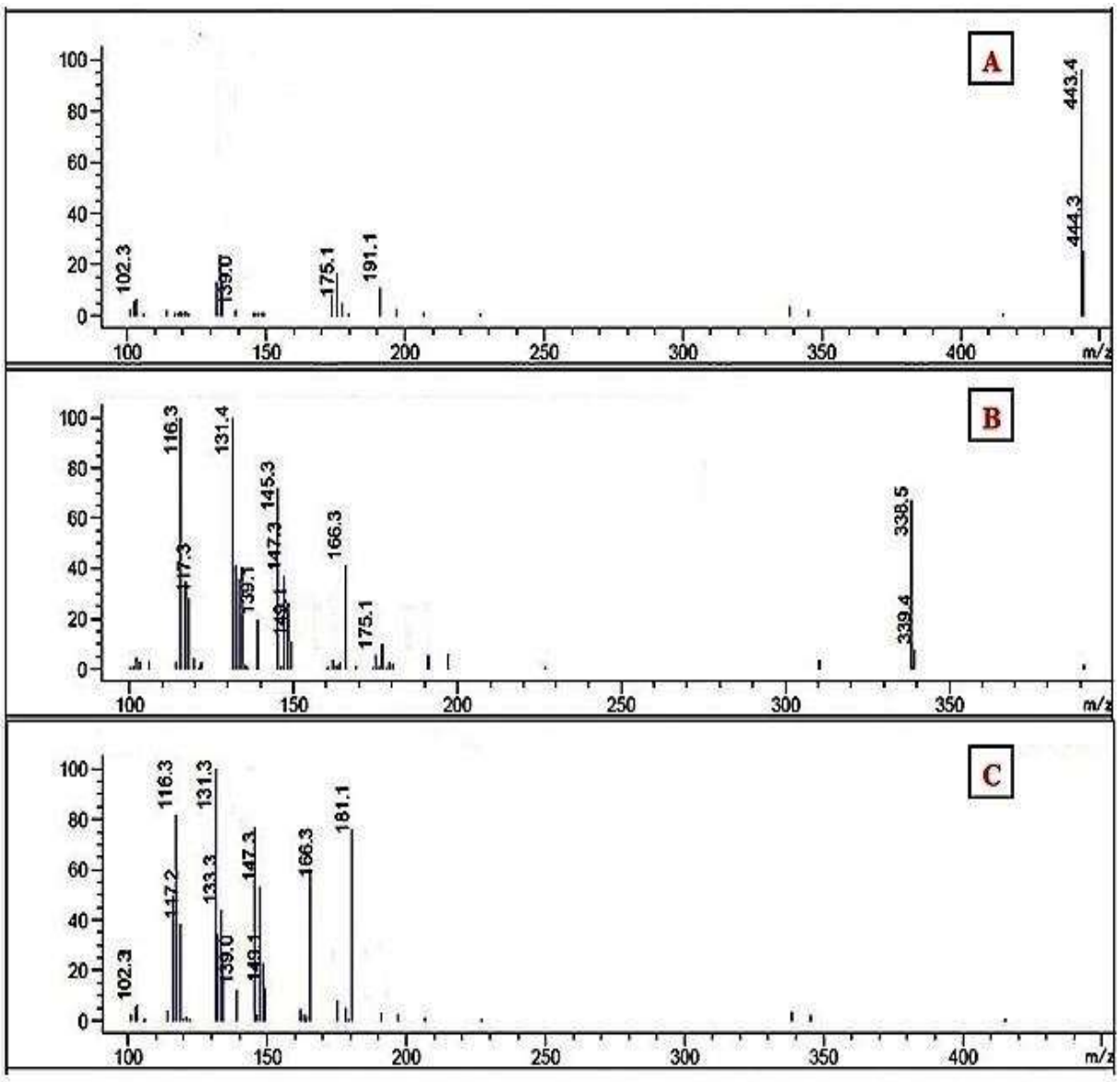

Figure 3.28: LC-MS spectra correspond to RhB (A), post-degraded end product of RhB after degradation in acidic (B), and alkaline medium (C)

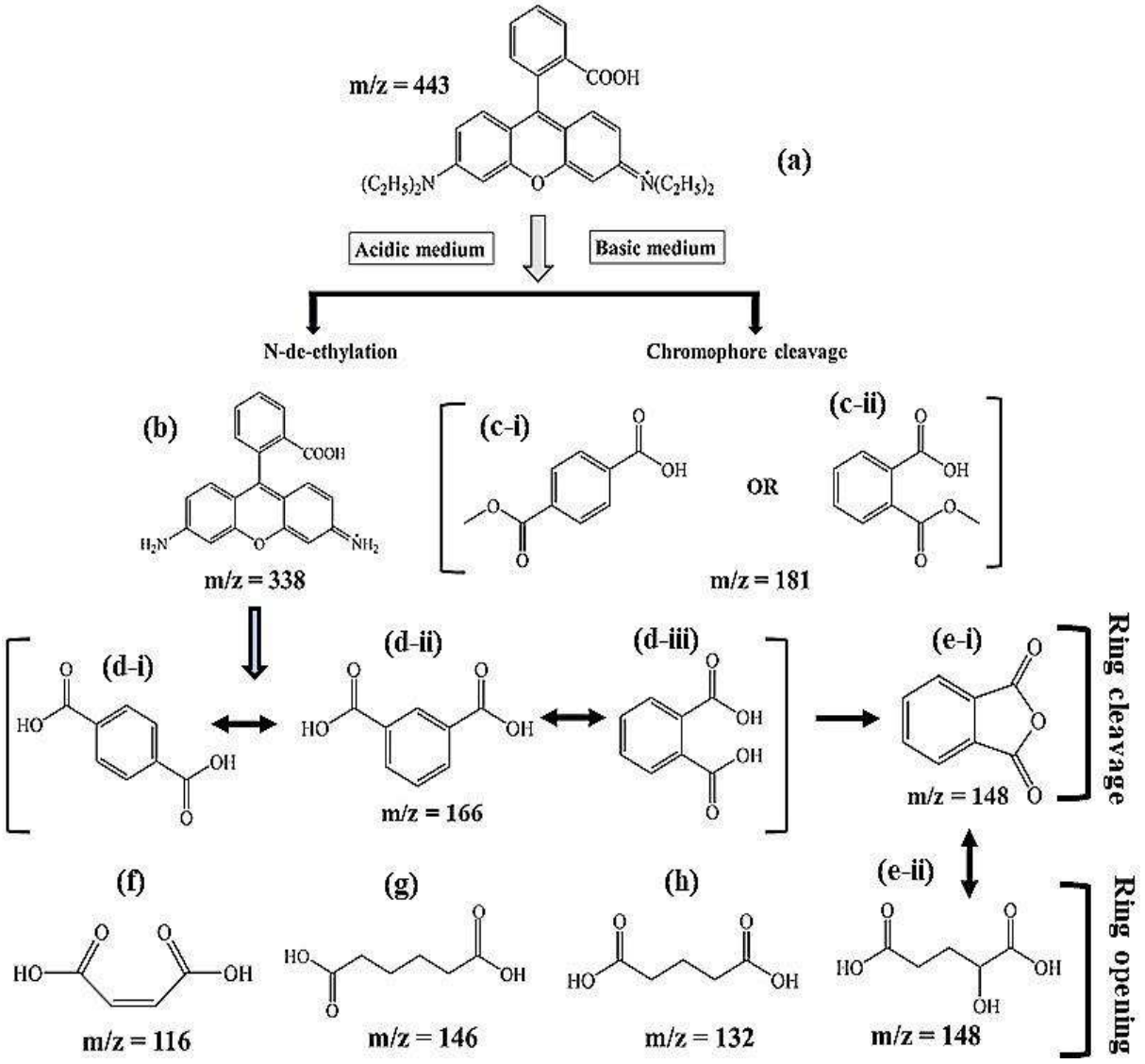

Figure 3.29: Photodegradation pathways of RhB in the presence of catalyst PBN and H_2O_2 via photo-Fenton process.

In addition to intermediate rhodamine (R), the successive degraded product observed at different m/z are listed in Table 3.4 exposed the plausible photodegradation pathways, as presented in Fig. 3.29. The small peak area of the N-deethylated products in the ion chromatogram (Fig. 3.28 B) revealed the existence of photodegradation over PBN catalyst surface that dominates the cleavage of whole conjugated Rhodamine (R) structure.

Untreated and PBN assisted photo-degraded RhB aqueous solutions were elected to perform the COD (Chemical Oxygen Demand) study. The Ferrous ammonium sulfate method (FAS) based on titration was used to determine the extent of mineralization and their non-toxic impact compared to the untreated dye toxicant. The resulting outcome

Table 3.4: Organic end product identified from LC-MS spectrum after photodegradation of RhB.

Product	m/z	Formula	Name
a	443	$C_{28}H_{31}C_1N_2O_3$	Rhodamine B
b	338	$C_{20}H_{15}C_1N_2O_3$	Rhodamine
c-i	181	$C_9H_8O_4$	4-(methoxycarbonyl)benzoic acid
c-ii	181	$C_9H_8O_4$	2-(methoxycarbonyl)benzoic acid
d-i	166	$C_8H_6O_4$	Terephthalic acid
d-ii	166	$C_8H_6O_4$	Iso phthalic acid
d-iii	166	$C_8H_6O_4$	Phthalic acid
e-i	148	$C_8H_4O_3$	Phthalic anhydride
e-ii	148	$C_5H_8O_5$	2-hydroxypentanedioic acid
f	146	$C_4H_4O_4$	Maleic acid
g	132	$C_6H_{10}O_4$	Adipic acid
h	116	$C_5H_8O_4$	Glutaric acid

showed that the COD demand for water containing untreated RhB molecules was very high (160 mg/L). However, a low value of COD was achieved to 56 mg/L by using PBN with H_2O_2 under solar light irradiation. The low COD value concerning catalyst treated RhB (20 ppm) indicates that the organic intermediate formed during photodegradation underwent oxidation and converted into carbon dioxide (CO_2) and water (H_2O) molecules. It also designated that organic intermediates produced throughout the photo-Fenton process underwent 65% of mineralization and convert into less toxic end products. The EPR spectroscopy, with spin-trapping agents DMPO and TEMPO, was used to identify the production of short-lived free radicals, i.e, $OH^{\bullet}$ and $O_2^{\bullet}$ generated by photo-Fenton catalyst under solar light irradiation. The quartet lines with 1:2:2:1 intensity corresponding to DMPO-OH adduct (Fig. 3.30A) and triplet of 1:1:1 to TEMPO-O_2 adduct (Fig. 3.30B), which confirm the production of $OH^{\bullet}$ and $O_2^{\bullet}$ radical in the solution throughout the degradation process (Madden et al., 2001; Punta et al., 2010). The above analytical outcome tentatively proposed the plausible mechanism for solar light induced RhB degradation process, via free radicals formation, using H_2O_2 in the presence of PBN catalyst.

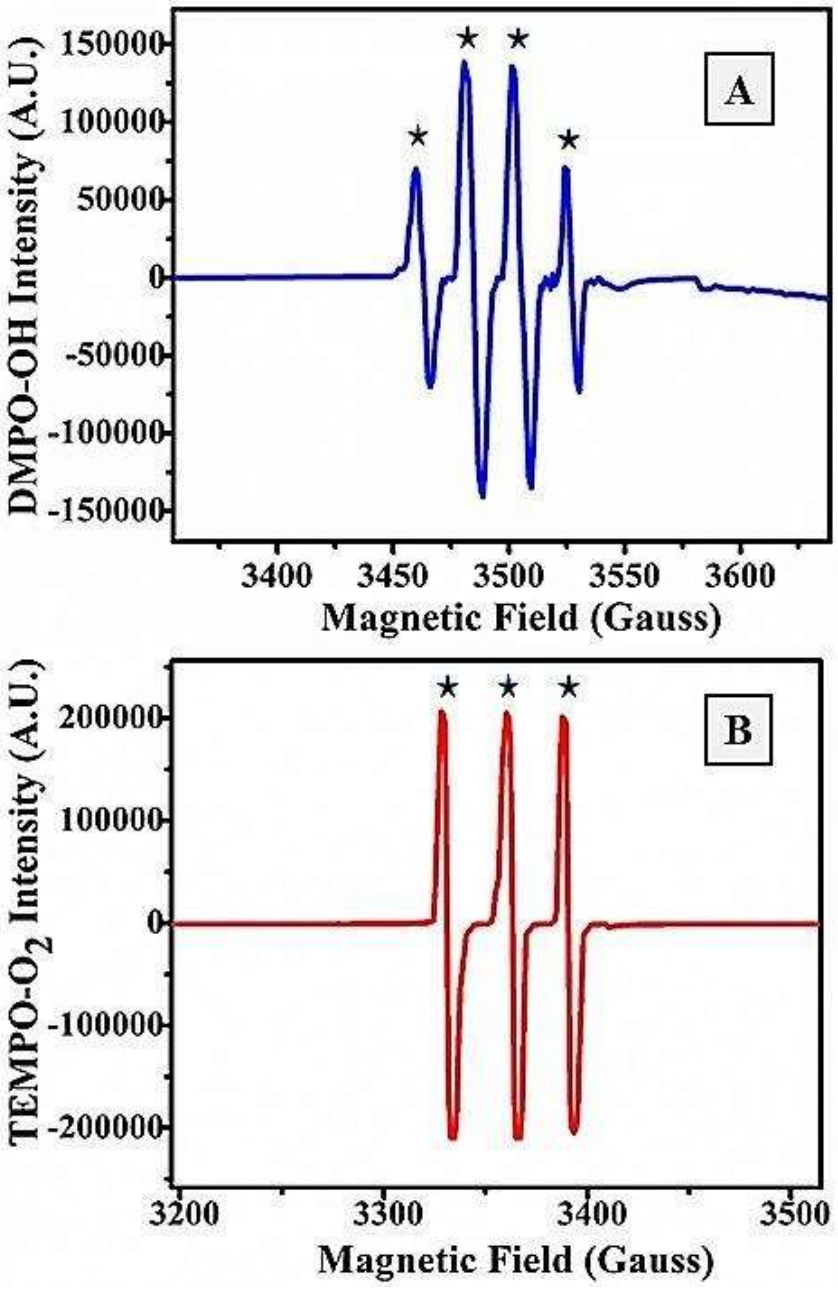

Figure 3.30: EPR spectra of DMPO-OH adduct of intensity 1:2:2:1 (A), and TEMPO-O_2 adduct of intensity 1:1:1 (B) corresponds to generated hydroxyl and superoxide radicals throughout photo-Fenton process.

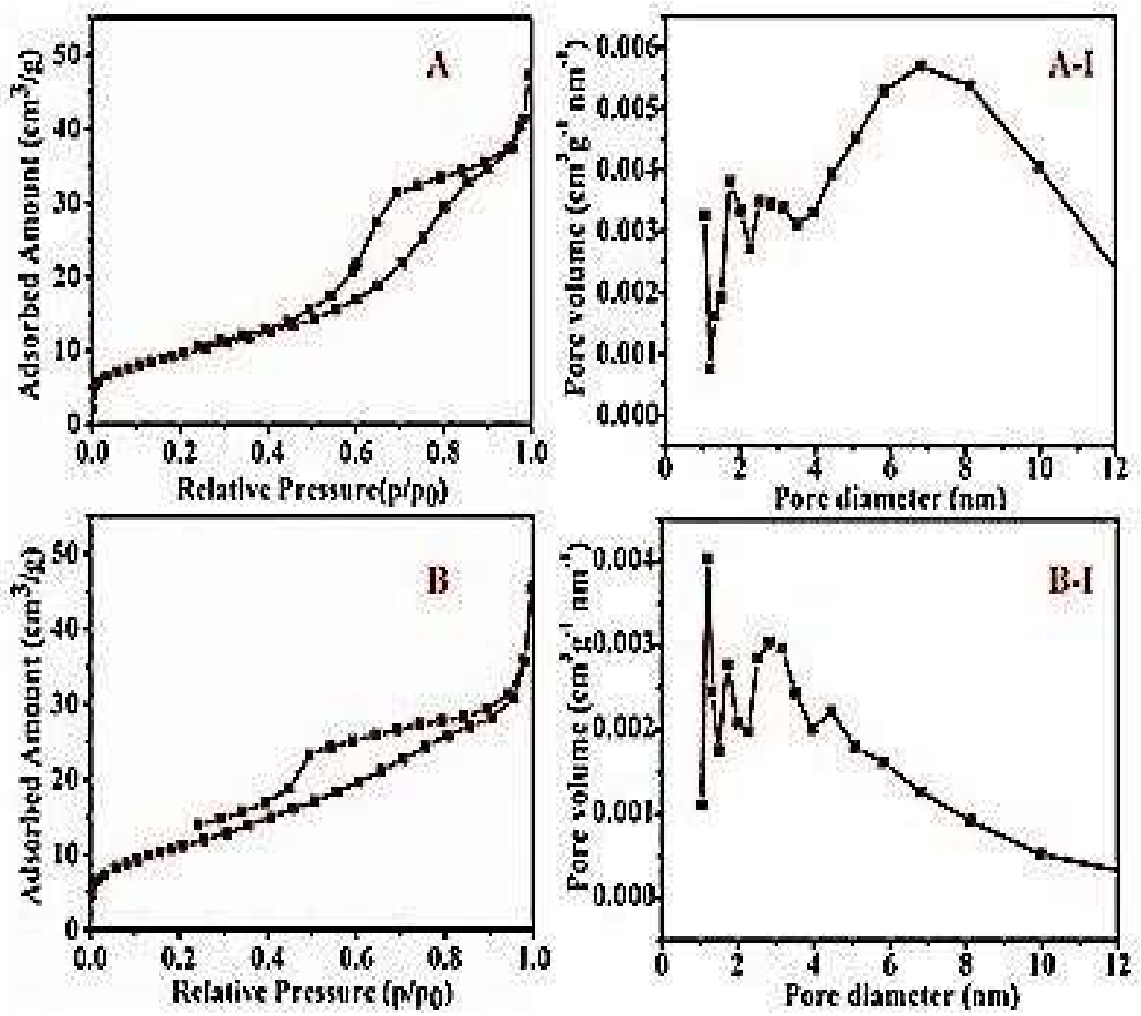

Figure 3.31: N_2 adsorption-desorption isotherms of unused (A), and recycled PBN catalyst (B). And BJH plot displaying pore diameter distribution curve for unused (A-I) and recycled PBN catalyst (B-I).

3.3.4 BET surface area analysis of unused and recycled catalyst

The specific surface area and pore diameter of as-synthesized catalyst was thoroughly investigated through BET analysis. The N_2 adsorption−desorption isotherms for unused PBN and recycled catalyst have been obtained at similar condition (Fig. 3.31(A,B)). The adsorption-desorption curve of unused catalyst (Fig. 3.31A) indicates a type-IV isotherm with the specific surface area of 34.3 m^2/g and a pore of 7.14 nm diameter (Fig. 3.31(A-I)). However, after their active participation in dye degradation process sort of decrease in surface area (31.87) (Fig. 3.31B) and in pore diameter (5.42 nm) was observed (Fig. 3.31 (B-I)) through the desorption-adsorption and BJH curve. The lowering in surface and pore volume was probably caused by consequence of nanoparticles agglomeration throughout the degradation process that leads to a reduction in pore diameter and specific surface area.

3.3.5 Anticipated degradation mechanism of photo-Fenton process

Coordination polymer PB comprised of iron metal centers linked by cyanide bridges in a rock-salt structure (Verdaguer and Girolami, 2005). Additionally, each iron centers Fe(II) and Fe(III) exist in low spin $(t_{2g})^6C(^1S)$ and high spin $(t_{2g})^3N\ (e_g)^2)N(^6S)$ configuration respectively in the PB framework (Robin, 1962). Each iron site has at least five electrons in their equivalent hole. Though at elevated temperature the additional valance electron of carbon hole is not fully localized on the metal centers (Robin and Day, 1968). The energy required to overcome this electronic transition from carbon hole to nitrogen hole defines the nanomaterial's band gap. The band gap of all synthesized PBN were calculated from quantum mechanics energy equation ($E = hc/\lambda$) using their corresponding absorption spectrum and recorded in Table 3.5 (Stanford et al., 2014).

The magnitude of this gap is such that it typically absorbs red end of visible spectrum leading to strong metal-to-metal charge-transfer (MMCT) transition which displays bright blue colour. Consequently, on solar light irradiation, the valance electron of carbon hole is activated by a photonic energy ($h\nu$) and execute charge transfer transition represented as Step 1:

Step 1. Photochemical reaction

$$[Fe^{2+}-C-N]Fe^{3+}+h\nu \rightarrow [Fe^{3+}-C-N]Fe^{2+}$$

Step 2. Photo-Fenton process at pH-3

$$Fe^{2+}[-NC-Fe^{3+}]+H_2O_2 \rightarrow Fe^{3+}[-NC-Fe^{3+}]+OH^{\bullet}+OH^{-} \qquad (K=76M^{-1}S^{-1})$$

Step 3. Pollutant degradation

$$OH^{\bullet}+RhB \rightarrow Degraded\ \ product \qquad (K=10^{7}-10^{10}M^{-1}S^{-1})$$

Step 4. Regeneration of catalyst

$$(I) \qquad H_2O_2+OH^{\bullet} \rightarrow HO_2^{\bullet}/O_2^{\bullet-} \qquad (K=3.3\times10^{7}M^{-1}S^{-1})$$

$$(II) \quad Fe^{3+}[-NC-Fe^{3+}]+HO_2^{\bullet}/O_2^{\bullet-} \rightarrow Fe^{3+}[-NC-Fe^{2+}]+O_2 \qquad (K=1.2\times10^{6}M^{-1}S^{-1})$$

$$(III) \quad Fe^{3+}[-NC-Fe^{3+}]+H_2O_2 \rightarrow Fe^{3+}[-NC-Fe^{2+}]+H_2O+HO_2^{\bullet} \qquad (K=0.01M^{-1}S^{-1})$$

The photo-Fenton process, composing complex Fe^{+2}/ Fe^{+3} reacting immediately to in-situ present H_2O_2 and furnished enormous hydroxyl radicals formation (K = 76 M^{-1} S^{-1}) as revealed in Step-2. The photo-Fenton process generated highly reactive hydroxyl radicals that offer the attack to the central carbon of dye before degradation. Most of the photo-generated hydroxyl radical successively react with dissolved organic pollutant RhB according to the above mentioned reaction sequence (step 3). Besides, the H_2O_2 similarly scavenges the Fenton process generated $OH^{\bullet}$ (Step-4 (I)), but yield $HO_2^{\bullet}$/ $O_2^{\bullet-}$ that enhances the recycling of Fe^{+3} to Fe^{+2} (faster process) as shown in reaction sequence (Step-4 (II)). The oxidized Fe^{+3}/Fe^{+3} also suggested to proceed with another molecule of H_2O_2 and tended to reduce itself as Fe^{+3}/ Fe^{+2} (Slow process) to further contribute into subsequent degradation process as shown in Step-4(III). Therefore, the $OH^{\bullet}$ scavenging by H_2O_2 could partially retard the overall Fenton process depending on the stoichiometric H_2O_2/Fe ratio (Reeser et al., 2009). However, the conversion efficiency of Fe (III) to Fe (II) accomplished through step (4) eliminating Fe^{+3} ability to act as scavengers and

enhances the reaction rate via continuous production of radicals (Xue et al., 2009; Zanta et al., 2010). The whole information attributed to the excellent photocatalytic activity that PBN possessed moreover in the acidic condition.

Table 3.5: Band gap analysis of all synthesized Nanoparticles.

Sample	λmax	E (eV)
PBN_1	681.82	1.822
PBN_2	682.83	1.819
PBN_3	683.54	1.817
PBN_4	684.71	1.814

3.3.6 Assessment of photo-Fenton process over polluted river water

Many industries, countless tanneries, chemical plants, textiles mills established on the bank of the Ganga, contribute to the pollution by discharging untreated waste into it. From the application point of view, the photodegradation study was performed on polluted river water to find out the photochemical response of Fenton complex (PBN+H_2O_2). For the degradation process, an adequate amount of RhB (10 ppm), PBN and H_2O_2 were added accordingly into the collected polluted water (50 ml) and allowed to irradiateunder solar light irradiation. It was observed that PBN+ H_2O_2 system lead to complete photodegradation (99%) of RhB (10 ppm) in only 1.5 min. However, some sort of delay (3 min) observed was probably due to presence of contaminated salts, such as Na_2SO_4 and $NaHCO_3$. The polluted industrial water contains interfering substances such as sulphate, carbonate, bicarbonate anions, and some dissolved organic substances which itself act as scavengers for in-situ generated hydroxyl radical and produces less efficient anions as follows;

$$SO_4^{2-} + OH^{\bullet} \rightarrow SO_4^{\bullet -} + OH^{\bullet}$$

$$CO_3^{2-} + OH^{\bullet} \rightarrow CO_3^{\bullet -} + OH^{\bullet}$$

$$HCO_3^{2-} + OH^{\bullet} \rightarrow CO_3^{\bullet -} + OH^{\bullet}$$

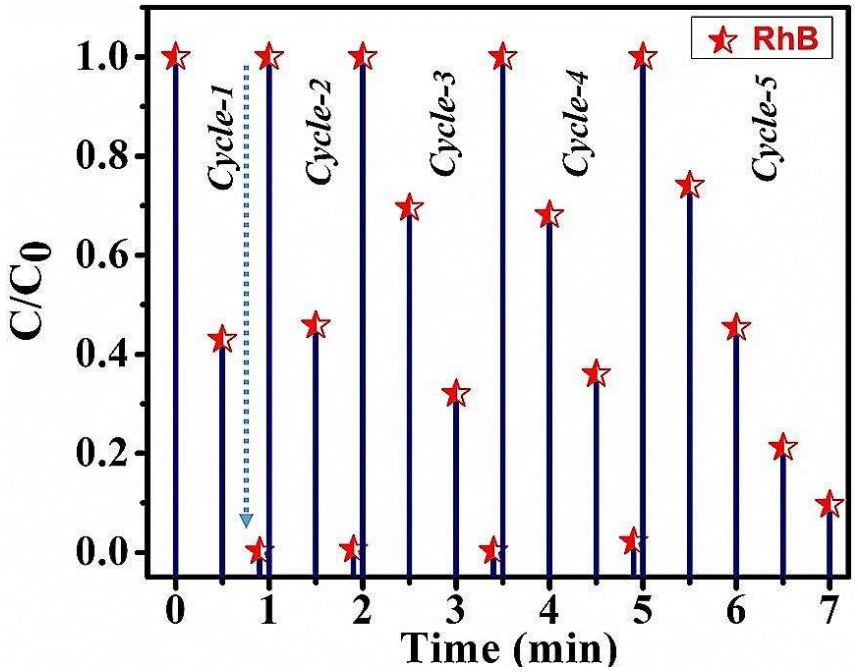

Figure 3.32: Study of recyclability of photo-Fenton catalyst via five subsequent repetitive cycles of RhB (10ppm) degradation.

3.3.7 Study of recyclability of catalyst after dye degradation

Recyclability and stability of the catalyst is essential aspect from the industrial point of view. The photo-Fenton catalyst PBN repeatedly reused in six subsequent degradation process. And it was found that photocatalyst efficiency remained highest (99%) in the first three cycles while after 4th, the loss in productivity was observed (Fig. 3.32). The sequential decrease in degradation percentage as well as in the rate was probably observed due to the following reason; (i) The absence of unoccupied active site at the PBN surface for unadsorbed RhB molecule. (ii) The high coloured solution of concentrated dye creates interference of photons to reach the surfaces of the nanoparticles. (iii) The generated hydroxyl radical via photo-Fenton process was reacted rapidly with unreacted bulk RhB molecule or formed intermediate that contracted the rate and efficiency (Lops et al., 2019).

3.3.8 Characterization of catalyst after post-degradation

After photo catalysis the PBN was separated via centrifugation and undergo TEM and FTIR analysis to analyze the impact of photodegradation on it. The presence of char-

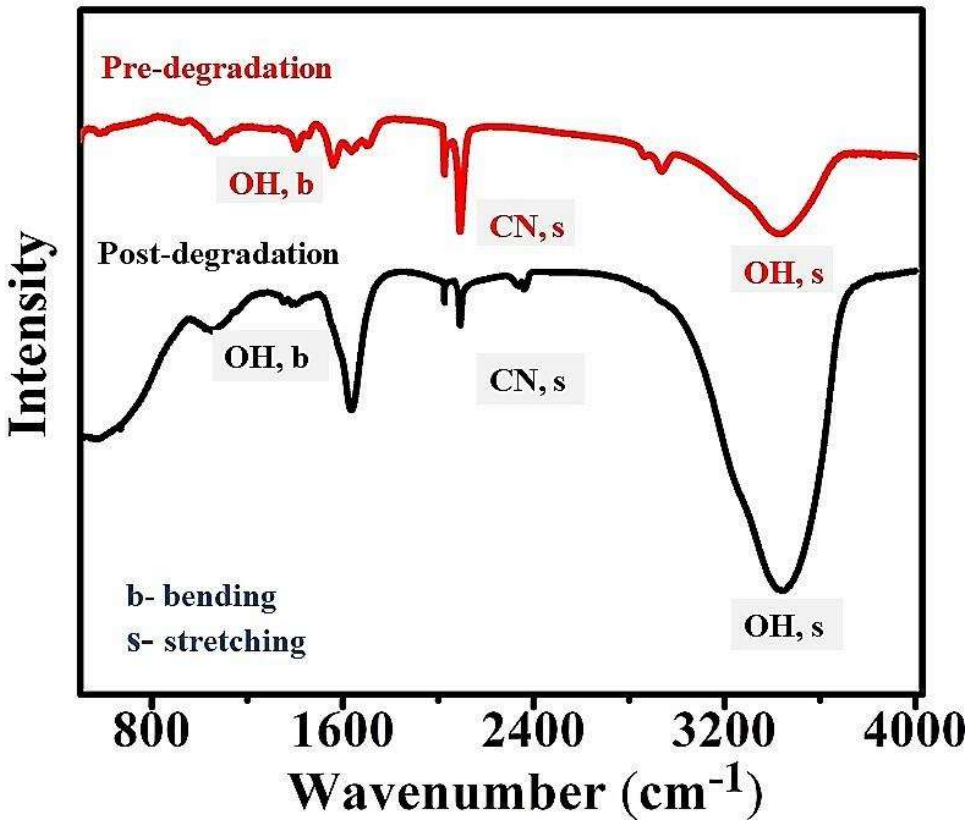

Figure 3.33: Comparative study of regenerated catalyst with unused one via ATR technique, after repetitive (five times) photodegradation process.

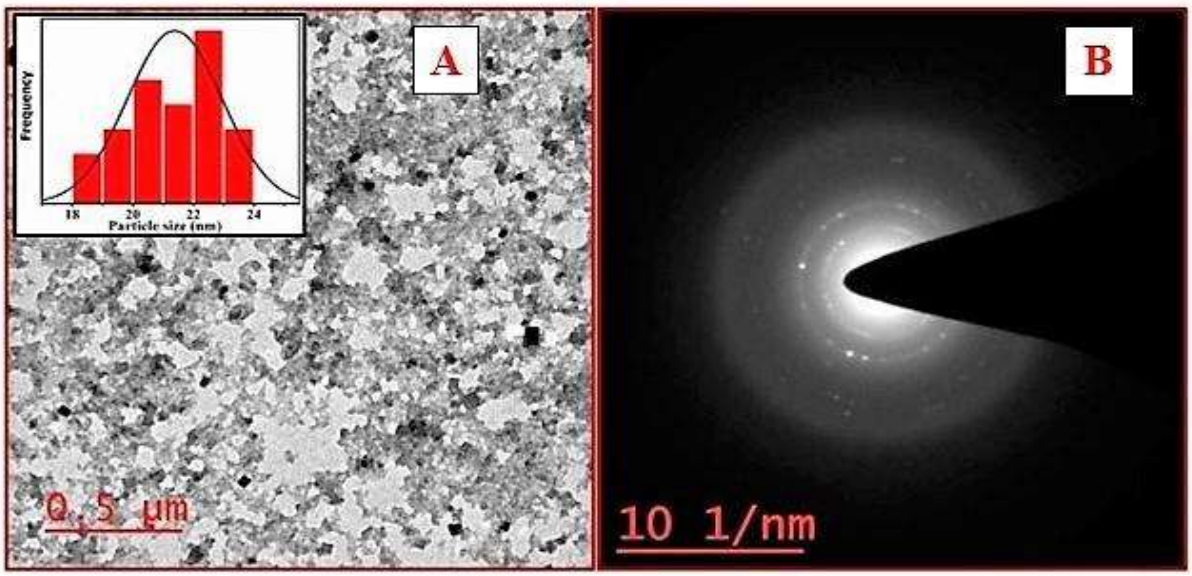

Figure 3.34: TEM image (A) and corresponding SAED (B) of reprocessed PBN_4 after repetitive (five times) photodegradation process. The histogram (in the inset of A) revealed the size of recycled nanoparticles.

acteristics CN starching peak (Fig. 3.33) confirmed the association of ligand with their respective iron centers. The TEM images of corresponding recoverable catalyst show growth in particle size as shown in Fig. 3.34A. The kind of size increment (22 nm) observed was attributed due to an agglomeration of particles as the PBN nanoparticle tend to come closer during degradation. This size addition is also answerable for the slow rate of degradation after repetitive cycles. Crystallinity of nanoparticle slightly decreases as observed through SAED pattern (Fig. 3.34B).

Table 3.6: Comparative study of previously reported system with this catalyst.

System	Targeted Dye	Source of Energy	Rate constant	References
BiOCl/g-C_3N_4	RhB	Visible Light	0.041 min^{-1}	Zhang et al., 2019
Ag_3PO_4@$MgFe_2O_4$	RhB	Visible Light	0.1370 min^{-1}	Zhou et al., 2018
Fe-Co	RhB	Heating	0.058 min^{-1}	Gong et al., 2017
Co-TiO2	RhB	Light Irradiation	0.07464 min^{-1}	Chen et al., 2013
PBN	RhB	Solar light	0.9253 min^{-1}	This work

3.4 CONCLUSION

Chemical reduction method successfully synthesized PBN of different size (13-53 nm) and morphologies such as; nano-cubes and nano-sphere using cyclohexanone with different EETMSi concentration. The degradation process was conducted by several means; RT, UV-radiation, solar light, and in heating condition. In particular, photodegradation method attempted individually with PBN or H_2O_2 in the solar irradiation shows the quiet amount of degradation. The advanced photo-Fenton process accomplished with different nano-sized PBN simplified the better performance of smaller particles than the larger ones. The result obtained in this current research for the degradation of RhB display efficiency of examined systems as follows; (PBN_4 + H_2O_2) >(PBN_3 + H_2O_2) >(PBN_2 + H_2O_2)>(PBN_1 + H_2O_2)>H_2O_2. The catalytic activity of above synthesized PBN towards photo-Fenton technique was found to favorable at pH 3. The different parameters; RhB, H_2O_2, and PBN were orderly varied to evaluate the kinetics and found to follow pseudo first-order kinetics. The outcome of these subsequent investigation reveals that the above process is more convenient at a large scale for complete removal of pollutant dye from wastewater. It shows complete degradation (100 %) endeavouring highest rate

constant (0.93 min^{-1}) as compare to the previous reported approach for RhB degradation (Table 3.6). The catalyst used in the following process is, non-hazardous, reliable and shows fast degradation using spontaneously accessible natural solar system. LC-MS analysis was performed to identify the degradation pathways for RhB degradation, meanwhile COD analysis concludes the 65% extent of mineralization. The recovered catalyst 'PBN_4' was further characterized by ATR and TEM to analyze the consequences of the photodegradation process over it.